

Water vapor millimeter wave foreign continuum: A Lanczos calculation in the coordinate representation

Q. Ma^{a)}

*NASA/Goddard Institute for Space Studies and Department of Applied Physics, Columbia University,
New York, New York 10025*

R. H. Tipping

Department of Physics and Astronomy, University of Alabama, Tuscaloosa, Alabama 35487

(Received 19 July 2002; accepted 4 September 2002)

The water vapor foreign-continuum absorption has been calculated theoretically from first principles for the millimeter wave spectral region as a function of frequency f and temperature T . The calculations are made using the Lanczos algorithm by writing the resolvent operator $(\omega - \mathcal{L})^{-1}$ as continued fractions. In order to guarantee the quick convergence of the continued fractions, the line space of H_2O is divided into two subspaces: one consists of the positive resonance lines and the other the negative ones. By ignoring the coupling between them, $(\omega - \mathcal{L})^{-1}$ is expressed as a sum of two continued fractions. The parameters appearing in each of the fractions are functions of the matrix elements of powers of the Liouville operator \mathcal{L} between the starting vectors spanning the corresponding subspaces. In the present work, we have taken into account all powers of \mathcal{L} up to 5. With the coordinate representation in which the orientations of the $\text{H}_2\text{O}-\text{N}_2$ collision pair are chosen as the basis functions in Hilbert space, the anisotropic interaction potential is diagonal, and calculations of the matrix elements are transformed to multidimensional integrations. The latter are evaluated with the Monte Carlo method. In order to reduce the lengthy calculations, we assume that the anisotropic potential has rotational symmetry about the Z axis of H_2O , and consists of the long-range dipole-quadrupole part and a short-range repulsive site-site model. Once the parameters of the continued fractions are known, one can calculate the poles and residues and then carry out the ensemble average over the translational motion. Within the quasistatic approximation, one can treat the latter classically and obtain contributions to the absorption coefficient at the poles. Finally, the absorption coefficient at frequency f can be derived by an interpolation method. The results are fitted to a simple function of f and T , and are compared with experimental data and with two different versions of Liebe's empirical model. In general, the theoretical results are in good agreement with the experiment. Meanwhile, the magnitudes of the theoretical absorption are between those of the 1989 and 1993 versions, but the temperature dependence is closer to the latter one. © 2002 American Institute of Physics. [DOI: 10.1063/1.1516792]

I. INTRODUCTION

A good knowledge of the water vapor millimeter wave foreign-continuum absorption is important for atmospheric applications, especially in dry air environments. At present, our understanding of the problem is not satisfactory. Laboratory measurements of the foreign continuum made by different groups differ by large amounts and various empirical models proposed differ significantly from each other.¹ Meanwhile, there is a lack of theoretical work heretofore from which one is able to predict the millimeter wave foreign continuum quantitatively well. Collision-induced absorption (CIA) has been proposed to be partly responsible for this continuum,² but there is no unambiguous laboratory evidence or theoretical calculations to support this assertion. On the other hand, although the recent far-wing line shape theory works well in calculating continuum absorptions for the infrared spectral region,³ its applicability in the millime-

ter wave region is questionable. The main reason for this is not the far-wing line shape theory itself, but the band average approximation,⁴ a usual procedure introduced to simplify calculations. There are some alternative theoretical methods available to calculate the millimeter wave continuum. One is so-called "third-order linear absorption" which has been applied for calculating the self-continuum.⁵ But this method is not applicable for the foreign continuum, at least for that caused by the $\text{H}_2\text{O}-\text{N}_2$ collision pairs, because it is limited to cases in which two interacting molecules undergo transitions by sharing one photon energy cooperatively. The second is the Lanczos algorithm, which was used successfully to calculate the millimeter wave self-continuum.⁶ With the Lanczos algorithm, we showed that one can write the spectral density as a continued fraction, and using the lowest-order truncation, we can calculate the absorption. However, an attempt to apply it for calculating the dominant contribution to the foreign continuum in the atmosphere caused by the $\text{H}_2\text{O}-\text{N}_2$ collision pairs has not been carried out. Because the molecules are not identical, there is no contribution to the

^{a)}Electronic mail: qma@giss.nasa.gov

absorption from the lowest-order truncation of the continued fractions. As shown in the next section, there are major problems encountered when one considers higher-order truncations.

A breakthrough for this problem arose from our far-wing line shape research. In the past few years, we have developed a first-principles far-wing line shape formalism and applied it to H_2O continuum absorption in the infrared spectral region. In order to overcome convergence problems, we introduced the coordinate representation in which the eigenfunctions of the orientations of the two interacting molecules are chosen as the complete set of basis functions in Hilbert space.^{7,8} With this representation, the interaction potential is diagonal, summations over states become multidimensional integrations over the continuous angular variables, and as many states as desired can be included in the calculations. The convergence criterion is transformed to the feasibility of calculating these integrations, and the latter can be successfully evaluated using the Monte Carlo method.³ Although the success of our far-wing line shape formalism in predicting the infrared continua does not help us directly to solve the millimeter problem, it turns out that the coordinate representation and the Monte Carlo method are two powerful tools that enable us to apply the Lanczos algorithm successfully for calculating the millimeter wave foreign continuum.

The paper is organized in the following way. In Sec. II, we discuss the general formalism for the calculation of the absorption coefficient. In Sec. II A, we briefly review the relation of the absorption coefficient to the spectral density, and express the latter in terms of traces over the internal and translational degrees of freedom for a pair of interacting molecules. In Sec. II B, we describe the Lanczos algorithm for writing the trace of the internal degrees in terms of a continued fraction. Explicit expressions for the parameters in the fraction up to third order are given in terms of the matrix elements of powers of the Liouville operator, \mathcal{L}^n up to $n = 5$, between the starting vector. In Sec. II C, we discuss the necessity to divide the whole line space into two subspaces involving the positive and negative resonance lines, respectively, and to express the trace of the internal degrees as a sum of two corresponding continued fractions. Ignoring the Liouville operator for the interaction potential, \mathcal{L}_1 , we obtain explicit results for the parameters in the fractions and find that there is no millimeter wave continuum. In Sec. II D, we consider the matrix element of \mathcal{L}_1 in the subspace constructed by the positive resonance lines. By introducing the coordinate representation, we can write this as a nine-dimensional integral over the angular degrees of freedom of the pair before and after the transition. However, from symmetry, this matrix element is zero; thus, to get finite contributions one has to consider higher powers of $\mathcal{L}(\equiv \mathcal{L}_a + \mathcal{L}_1)$. The latter is the most time-consuming computation in the present study and the details of how these are calculated or approximated are given in Sec. II E. Then, using these results one can easily obtain the two continued fractions. From these the poles and residues can be determined, and the procedure is discussed in Sec. II F. In Sec. II G, the trace over the translational degrees is treated classically as an ensemble average over the separation r between the two molecules,

and this yields contributions to the absorption coefficients at the poles. An interpolation scheme is discussed, which enables us to calculate the absorption coefficient at any frequency of interest. In Sec. II H, we discuss the model for the interaction potential used. The anisotropic part of this potential is assumed to have rotational symmetry about the Z axis of H_2O , and consists of the long-range dipole–quadrupole part and a short-range repulsive site–site model. The isotropic part of the interaction potential necessary to carry out the ensemble average over the translational coordinate r , is modeled by a Lennard-Jones, and numerical parameters are given. In Sec. II I, we present the numerical results for the absorption coefficient, $\alpha(f)$, in units of dB/km, as a function of frequency f in GHz for several temperatures. We derive a simple fitting formula for the theoretical results and discuss the comparisons with experimental data and with the widely used MPM89⁹ and MPM93¹⁰ empirical models, two versions of the millimeter wave propagation model developed by Liebe.

In Sec. III, we first discuss the meaning of the results for the millimeter wave absorption obtained from the Lanczos method. The possible importance of CIA is discussed briefly, but we show that one is able to explain this continuum well without relying on appreciable CIA. We compare the Lanczos method with the far-wing line shape theory, and although they arise from the same physical mechanism, they use different methods to account for contributions to the absorption and are subjected to different limitations. The latter works well to predict absorptions in the infrared spectral region, but the former is more applicable in the millimeter wave region. We conclude by discussing some possible improvements and extensions of the present results, including a more general interaction potential without the assumption of cyclic coordinates, and the inclusion of higher-order terms in the continued fractions. While these refinements are possible, we feel that it is first necessary to test how well the present theoretical formula works in atmospheric applications.

II. THE GENERAL FORMALISM

A. The absorption coefficient and spectral density

As is well known, the absorption of radiation at frequency ω (cm^{-1}) per unit volume of a gaseous sample in thermal equilibrium at temperature T is characterized by the absorption coefficient $\alpha(\omega)$:

$$\alpha(\omega) = \frac{4\pi^2}{3\hbar c} \omega (e^{\beta\hbar\omega} - 1) F(\omega). \quad (1)$$

The spectral density $F(\omega)$ is the Fourier transform of the correlation function $C(t)$ of the dipole moment operator; that is,

$$F(\omega) = \frac{1}{\pi} \text{Re} \int_0^\infty e^{i\omega t} C(t) dt, \quad (2)$$

and

$$C(t) = \text{Tr}(\boldsymbol{\mu}^\dagger e^{-iHt} \rho \boldsymbol{\mu} e^{iHt}), \quad (3)$$

where $\boldsymbol{\mu}$ is the dipole moment operator of the sample and ρ is the density matrix. Then, $F(\omega)$ can be given by

$$F(\omega) = -\frac{1}{\pi} \text{Im Tr} \left(\boldsymbol{\mu}^\dagger \frac{1}{\omega - \mathcal{L}} \boldsymbol{\rho} \boldsymbol{\mu} \right),$$

or alternatively by¹¹

$$F(\omega) = -\frac{1}{\pi} \text{Im Tr} \left(\boldsymbol{\mu}^\dagger \sqrt{\boldsymbol{\rho}} \frac{1}{\omega - \mathcal{L}} \sqrt{\boldsymbol{\rho}} \boldsymbol{\mu} \right), \quad (4)$$

which is preferable to pursue our further study. In these expressions, the Liouville operator \mathcal{L} associated with the total Hamiltonian H is defined as

$$\mathcal{L}A \equiv HA - AH, \quad (5)$$

where A is an arbitrary operator in Hilbert space.

In the present study, we only consider low-pressure cases in which both the water vapor density and the nitrogen buffer density are low. Based on the binary collision approximation, one can further focus on a single $\text{H}_2\text{O}-\text{N}_2$ pair and neglect its correlation with others. As a result, the absorption coefficient $\alpha(\omega)$ of the whole gas sample can be expressed as

$$\alpha(\omega) = \frac{4\pi^2}{3\hbar c} n_{\text{pair}} \omega (e^{\beta\hbar\omega} - 1) F(\omega), \quad (6)$$

where n_{pair} is the number density of pairs and it is proportional to the product of the pressures of H_2O and N_2 ; $F(\omega)$ is the spectral density of the pair whose expressions are the same as Eqs. (2) and (4), except all the quantities belong to the pair only. For simplicity, we do not introduce new symbols for the two-molecule system. For later convenience, the Liouville operator L can be expressed as the sum of its components:

$$\mathcal{L} = \mathcal{L}_a + \mathcal{L}_b + \mathcal{L}_1, \quad (7)$$

corresponding to the unperturbed H_2O molecule, the unperturbed N_2 , and the anisotropic interaction between H_2O and N_2 . We note that because the isotropic interaction $V_{\text{iso}}(r)$ commutes with all other operators, one can exclude $V_{\text{iso}}(r)$ from \mathcal{L}_1 . Based on the same reason, one can move $\rho_{\text{iso}}[\equiv \exp(-\beta V_{\text{iso}}(r))]$ introduced later anywhere in the trace.

In the present study, the frequencies of interest are only a few cm^{-1} , which are much smaller than the strong resonance line frequencies. As shown later, during collision processes, the anisotropic interaction can cause millimeter wave continuum absorptions when H_2O and N_2 have separations between 3.4 and 5 Å. It is well known that at this range, the whole interaction is rather weak and the anisotropic part is even weaker. Therefore, one can conclude that for cases of interest here not only $V_{\text{iso}}(r) < H_a$, but also $V_{\text{ani}}(r) < H_a$. We note that, based on the latter, we can draw another conclusion that $\mathcal{L}_1 < \mathcal{L}_a$, which will be used in our later discussions. Then, we can introduce the approximation $\rho \approx \rho_a \rho_b \rho_{\text{iso}}$ in Eq. (4) and, in addition, we can exclude the component \mathcal{L}_b from \mathcal{L} because H_b commutes with $\sqrt{\rho_a \rho_b \rho_{\text{iso}}} \boldsymbol{\mu}$. By dividing all degrees of freedom of the two interacting molecules into internal and translational degrees, we rewrite the expression for $F(\omega)$ as

$$F(\omega) = -\frac{1}{\pi} \text{Im Tr}_r \left\{ \rho_{\text{iso}} \text{Tr}_{ab} \left(\boldsymbol{\mu}^\dagger \sqrt{\rho_a \rho_b} \frac{1}{\omega - \mathcal{L}} \sqrt{\rho_a \rho_b} \boldsymbol{\mu} \right) \right\}. \quad (8)$$

In the above expression, the trace operator Tr_{ab} is over the internal degrees and the trace operator Tr_r is over the translational degrees. It turns out that to carry out Tr_{ab} is much more difficult than Tr_r . Therefore, we focus our attention on Tr_{ab} first and apply the Lanczos algorithm to solve the problem.

B. Lanczos algorithm

It is well known that the Lanczos algorithm is a useful technique in molecular dynamics. We do not describe this method in detail here; rather the reader is referred to the review by Moro and Freed, and references therein.¹² In line space, the Liouville operator \mathcal{L} and therefore the resolvent operator $(\omega - \mathcal{L})^{-1}$ are matrix operators; ordinary (in Hilbert space) operators (for instance, $\sqrt{\rho_a \rho_b} \boldsymbol{\mu}$) are vectors. One begins by defining a starting vector (in line space),

$$|1\rangle = |v\rangle / \sqrt{\langle v|v\rangle}, \quad (9)$$

where $|v\rangle \equiv \sqrt{\rho_a \rho_b} \boldsymbol{\mu}$, and from this, one generates a complete set of basis vectors $(|1\rangle, |2\rangle, \dots, |n\rangle, \dots)$ according to

$$\begin{aligned} \beta_2 |2\rangle &= (1 - P_1) \mathcal{L} |1\rangle, \\ \beta_3 |3\rangle &= (1 - P_2) \mathcal{L} |2\rangle, \\ &\dots \\ \beta_n |n\rangle &= (1 - P_{n-1}) \mathcal{L} |n-1\rangle. \end{aligned} \quad (10)$$

In these expressions, P_n are the projection operators,

$$P_n = \sum_{i=1}^n |i\rangle \langle i|, \quad (11)$$

and the quantities β_n are determined from the normalization requirement ($\langle n|n\rangle = 1$); these are given by

$$\beta_n = \langle n | \mathcal{L} | n-1 \rangle, \quad \text{for } n > 1. \quad (12)$$

The matrix representation of \mathcal{L} in line space given in the complete basis $(|1\rangle, |2\rangle, \dots)$ has the symmetric tridiagonal form whose off-diagonal elements are β_n ($n=1, 2, \dots$) and whose diagonal elements, α_n ($n=1, 2, \dots$), are given by

$$\alpha_n = \langle n | \mathcal{L} | n \rangle. \quad (13)$$

Then, one can write the inner trace of $F(\omega)$ in terms of a continued fraction,⁶

$$\begin{aligned} &\text{Tr}_{ab} \left(\boldsymbol{\mu}^\dagger \sqrt{\rho_a \rho_b} \frac{1}{\omega - \mathcal{L}} \sqrt{\rho_a \rho_b} \boldsymbol{\mu} \right) \\ &= \left\langle v \left| \frac{1}{\omega - \mathcal{L}} \right| v \right\rangle = \langle v | v \rangle \frac{1}{\omega - \alpha_1 - \frac{\beta_2^2}{\omega - \alpha_2 - \frac{\beta_3^2}{\omega - \alpha_3 - \dots}}}. \end{aligned} \quad (14)$$

It is worth mentioning that all quantities $\langle v | v \rangle$, α_n , and β_n appearing in the continued fraction expression are matrix el-

ements. However, except for $\langle v|v\rangle$, their values can vary. Because \mathcal{L}_1 depends on the separation r between the two molecules, α_n and β_n depend on r also. As shown later, the translational motion of two molecules can be treated classically; thus, one can consider r as a parameter here.

The continued fraction expression for $F(\omega)$ is the starting formula to carry out numerical calculations. In practice, one has to introduce a cutoff in Eq. (14) to limit fractions included and to make sure results obtained accordingly are converged. A simple convergence criterion is the requirement

$$\beta_n^2 \ll \alpha_{n-1} \alpha_n, \quad \text{for } n > 1. \quad (15)$$

The expressions for α_n and β_n^2 appearing explicitly in Eq. (14) can be given in terms of matrix elements of \mathcal{L} and its powers between the starting vector $|1\rangle$,

$$\alpha_1 = \langle 1|\mathcal{L}|1\rangle,$$

$$\beta_2^2 = \langle 1|\mathcal{L}^2|1\rangle - \alpha_1^2,$$

$$\alpha_2 = \frac{1}{\beta_2^2} (\langle 1|\mathcal{L}^3|1\rangle - 2\alpha_1\langle 1|\mathcal{L}^2|1\rangle + \alpha_1^3), \quad (16)$$

$$\beta_3^2 = \frac{1}{\beta_2^2} (\langle 1|\mathcal{L}^4|1\rangle - 2\alpha_1\langle 1|\mathcal{L}^3|1\rangle + \alpha_1^2\langle 1|\mathcal{L}^2|1\rangle) - \alpha_2^2 - \beta_2^2,$$

$$\alpha_3 = \frac{1}{\beta_3^2} \left\{ \alpha_2^3 - 2\langle 1|\mathcal{L}^3|1\rangle + 2\alpha_1\langle 1|\mathcal{L}^2|1\rangle + (\alpha_1 + 2\alpha_2)\beta_2^2 + \frac{1}{\beta_2^2} [\langle 1|\mathcal{L}^5|1\rangle - 2(\alpha_1 + \alpha_2)\langle 1|\mathcal{L}^4|1\rangle + \alpha_1(\alpha_1 + 4\alpha_2)\langle 1|\mathcal{L}^3|1\rangle - 2\alpha_1^2\alpha_2\langle 1|\mathcal{L}^2|1\rangle] \right\},$$

etc. As shown by Eq. (16), when the lowest-order cutoff is chosen, the continued fraction becomes simply $(\omega - \alpha_1)^{-1}$ and there is only one matrix element $\langle 1|\mathcal{L}|1\rangle$ required. For the next cutoff, one needs to calculate α_1 , β_2^2 , and α_2 . This implies that one needs to know $\langle 1|\mathcal{L}^2|1\rangle$ and $\langle 1|\mathcal{L}^3|1\rangle$ as well. If one goes one step further, β_3^2 and α_3 are needed and two additional matrix elements $\langle 1|\mathcal{L}^4|1\rangle$ and $\langle 1|\mathcal{L}^5|1\rangle$ are required. Because \mathcal{L}_a is the dominant part of \mathcal{L} , we can calculate the matrix elements $\langle 1|\mathcal{L}_a^n|1\rangle$ with $n = 1, 2, \dots$, first and treat contributions from \mathcal{L}_1 as corrections. We note that the former are independent of the parameter r while the latter are functions of r .

C. Two starting vectors and the matrix elements of \mathcal{L}_a^n

As a guide to go further, it is wise to do a simple test first. By neglecting contributions from \mathcal{L}_1 , we can easily evaluate α_1 , β_2^2 , α_2 , β_3^2 , and α_3 which are just five numbers. However, it turns out that the magnitudes of α_1 , α_2 , and α_3 are so small that they cause a failure of the convergence criterion, Eq. (15). It is the cancellation between positive resonance lines of H_2O and negative resonance ones that reduces their magnitudes significantly. Therefore, in order to guarantee the convergence, one can divide $|v\rangle$ (i.e., $|\sqrt{\rho_a\rho_b}\mu\rangle$) into two parts: $|v\rangle_+$ associated with the positive

resonance lines and $|v\rangle_-$ with the negative resonance ones. The physical meaning of this division is to separate an average over the whole band of H_2O into two averages: one over the positive resonance lines and the other over the negative resonance ones.

Based on this, we introduce two independent starting vectors: $|1\rangle_+$ and $|1\rangle_-$. Because \mathcal{L}_a , the dominant component of \mathcal{L} , does not mix $|1\rangle_+$ and $|1\rangle_-$ and, in general, energy gaps between two components belonging to $|1\rangle_+$ and $|1\rangle_-$, respectively, are larger than those within $|1\rangle_+$ or within $|1\rangle_-$, we expect that the coupling between them can be ignored in the calculations. Then, the inner trace of $F(\omega)$ can be expressed as a sum over two terms:

$$\begin{aligned} \text{Tr}_{ab} \left(\mu^\dagger \sqrt{\rho_a\rho_b} \frac{1}{\omega - \mathcal{L}} \sqrt{\rho_a\rho_b} \mu \right) \\ = {}_+\langle v | \frac{1}{\omega - \mathcal{L}} | v \rangle_+ + {}_-\langle v | \frac{1}{\omega - \mathcal{L}} | v \rangle_-. \end{aligned} \quad (17)$$

By following the same procedure as described above, we can rewrite each term as a continued fraction as in Eq. (14). Accordingly, there are two independent sets of α_n and β_n^2 to be evaluated. For simplicity, we do not introduce new symbols for quantities associated with $|v\rangle_+$ and $|v\rangle_-$. In addition, due to their similarity, it is unnecessary to repeat discussions for each case. We will only present formulas applicable for $|v\rangle_+$ and simply mention differences between $|v\rangle_+$ and $|v\rangle_-$.

The expression of the line space vector $|v\rangle_+$ is given by

$$\begin{aligned} |v\rangle_+ = \sum_{j\tau m} \sum_{j'\tau'm'} \sum_{ln} \{ \sqrt{g_\tau g_l} e^{-\beta[E(j,\tau) + E(l)]/2} \\ \times \langle j\tau m | \mu | j'\tau'm' \rangle / \sqrt{Q_a Q_b} \} |j\tau m ln\rangle \langle ln j'\tau'm'|, \end{aligned} \quad (18)$$

where $|j\tau m ln\rangle$ is a simple notation for $|j\tau m\rangle \otimes |ln\rangle$, g_τ and g_l are the nuclear spin degeneracy factors for H_2O and N_2 , Q_a and Q_b are the partition functions of H_2O and N_2 , respectively, and the summation over j' and τ' is limited to a range with $E(j',\tau') < E(j,\tau)$. We note that we have ignored contributions from vibrational bands of H_2O because they are not only weaker than the pure-rotational band, but also are farther away from the millimeter spectral region. We introduce a normalization constant M_+ , defined by

$$M_+ = \sum_{j\tau} \sum_{\{j'\tau'\}_+} (2j+1) g_\tau e^{-\beta E(j,\tau)} |\mu_{j\tau,j'\tau'}|^2 / Q_a, \quad (19)$$

where the summation over j' and τ' indicated by a symbol $\{j'\tau'\}_+$ is limited to a range with $E(j',\tau') < E(j,\tau)$. In the above expression, $\mu_{j\tau,j'\tau'}$, which are associated with the reduced dipole matrix elements, but exclude the magnitude μ of the dipole operator of H_2O , are given in the body-fixed frame of H_2O in which the dipole moment lies along its Z axis (i.e., the III' representation) by

$$\mu_{j\tau,j'\tau'} = \sqrt{(2j'+1)/(2j+1)} \sum_k U_{k\tau}^j U_{k\tau'}^{j'} C(j'1j,k0k), \quad (20)$$

where $C(j'1j,k0k)$ is a Clebsch–Gordan coefficient; $U_{k\tau}^j$ results from expressing $|j\tau m\rangle$, the wave functions of H_2O , in terms of an expansion of symmetric-top wave functions $|jkm\rangle$, viz.,

$$|j\tau m\rangle = \sum_k U_{k\tau}^j |jkm\rangle. \quad (21)$$

It is obvious that ${}_+\langle v|v\rangle_+ = \mu^2 M_+$. It is easy to derive expressions for ${}_+\langle 1|\mathcal{L}_a^n|1\rangle_+$ which are given by

$${}_+\langle 1|\mathcal{L}_a^n|1\rangle_+ = \frac{1}{M_+} \sum_{j\tau} \sum_{\{j'\tau'\}_+} (2j+1) g_{\tau} e^{-\beta E(j,\tau)} \times |\mu_{j\tau,j'\tau'}|^2 \{E(j,\tau) - E(j',\tau')\}^n / Q_a. \quad (22)$$

We note that the expressions for ${}_+\langle 1|\mathcal{L}_a^n|1\rangle_+$ are completely independent of N_2 .

We include all H_2O states up to $J_{\max}=26$ in our numerical calculations. We calculate M_+ from Eq. (19) and the matrix elements ${}_+\langle 1|\mathcal{L}_a^n|1\rangle_+$ from Eq. (22) for $T=296\text{ K}$. The former's value is $0.374\,900$ and the latter's values are 95.1928 cm^{-1} , $126\,80.7\text{ cm}^{-2}$, $2.165\,27 \times 10^6\text{ cm}^{-3}$, $4.468\,50 \times 10^8\text{ cm}^{-4}$, and $1.071\,06 \times 10^{11}\text{ cm}^{-5}$ for $n=1, 2, 3, 4$, and 5 , respectively. Accordingly, we obtain $\alpha_1 = 95.1928\text{ cm}^{-1}$, $\beta_2^2 = 3619.05\text{ cm}^{-2}$, $\alpha_2 = 169.562\text{ cm}^{-1}$, $\beta_3^2 = 8944.98\text{ cm}^{-2}$, and $\alpha_3 = 226.850\text{ cm}^{-1}$. Based on these values, it is easy to check that the convergence criterion is satisfied because $\beta_2^2/(\alpha_1\alpha_2) = 0.224$ and $\beta_3^2/(\alpha_2\alpha_3) = 0.233$.

We also calculate quantities associated with the starting vector $|1\rangle_-$ from formulas similar to Eqs. (18), (19), and (22), respectively, except the summations are carried out with $E(j',\tau') > E(j,\tau)$. The value of M_- obtained is $0.625\,100$ and the values of the matrix elements ${}_-\langle 1|\mathcal{L}_a^n|1\rangle_-$ with $n=1, 2, 3, 4$, and 5 are -116.535 cm^{-1} , $18\,878.2\text{ cm}^{-2}$, $-3.871\,09 \times 10^6\text{ cm}^{-3}$, $9.484\,21 \times 10^8\text{ cm}^{-4}$, and $-2.683\,76 \times 10^{11}\text{ cm}^{-5}$, respectively. The corresponding values of α_n and β_n^2 are $\alpha_1 = -116.535\text{ cm}^{-1}$, $\beta_2^2 = 5297.76\text{ cm}^{-2}$, $\alpha_2 = -198.902\text{ cm}^{-1}$, $\beta_3^2 = 12\,250.93\text{ cm}^{-2}$, and $\alpha_3 = -276.662\text{ cm}^{-1}$. Finally, the convergence check yields $\beta_2^2/(\alpha_1\alpha_2) = 0.229$ and $\beta_3^2/(\alpha_2\alpha_3) = 0.223$, respectively.

Based on these values, explicit expressions for $F(\omega)$ in terms of the two continued fractions are known. Then, one can easily find the poles of the fractions on the ω axis. For the lowest-order cut-off, there are two poles: $\omega = 95.1928\text{ cm}^{-1}$ and $\omega = -116.535\text{ cm}^{-1}$, one from each of the continued fractions, respectively. For the next order, there are four poles: $\omega = 61.6543\text{ cm}^{-1}$, 203.100 cm^{-1} and $\omega = -74.0896\text{ cm}^{-1}$, -241.348 cm^{-1} associated with $|1\rangle_+$ and $|1\rangle_-$, respectively. Then, for the next higher order shown explicitly in Eq. (14), there are six poles: $\omega = 46.1918$, 141.861 , and 303.552 cm^{-1} and $\omega = -55.9511$, -173.407 , and -362.742 cm^{-1} , respectively. Because there is no pole within the millimeter spectral region, it seems that without considering the interaction between H_2O and N_2 , there are no local line absorptions in this region at all. Clearly, the above statement

is not correct because there are a few relatively weak lines there. But, given the fact that most lines of the pure rotational band are located beyond the millimeter spectral region and that results from the Lanczos algorithm represent averaged effects mainly over these lines, our finding is consistent. This also indicates that it is the anisotropic interaction that plays a crucial role in causing the millimeter wave absorption.

By comparing the values of the poles given above, it is obvious that those associated with $|1\rangle_+$ and those with $|1\rangle_-$ are not symmetrically located about the origin of the ω axis. As shown by Fig. 5 presented later, the same finding remains true when contributions from \mathcal{L}_1 are included. This asymmetry results from the procedure used here to introduce $|v\rangle_+$ and $|v\rangle_-$ with which the original vector $|v\rangle$ is not evenly divided between them. It is worth mentioning that one can start from the symmetric correlation function $\tilde{C}(t) \equiv C(t + i\beta\hbar/2)$, which has the symmetry of $\tilde{C}(t) = \tilde{C}(-t)$ and follows the same procedures presented here, including introducing a new vector $|v\rangle$ and its two evenly divided components $|v\rangle_+$ and $|v\rangle_-$. We expect that the poles associated with the new starting vectors $|1\rangle_+$ and $|1\rangle_-$ will be symmetrically distributed along the ω axis.

D. Matrix element ${}_+\langle 1|\mathcal{L}_1|1\rangle_+$

Up to this stage, we have not faced serious obstacles but we have not achieved substantial progress either. In contrast, the next step, i.e., to calculate matrix elements involving \mathcal{L}_1 , becomes a big challenge. From the following analyses, one can understand why. First of all, let us consider the calculation of ${}_+\langle 1|\mathcal{L}_1|1\rangle_+$, which can be explicitly expressed in terms of Hilbert operators as

$${}_+\langle 1|\mathcal{L}_1|1\rangle_+ = \frac{1}{M_+} \langle j\tau m | \mu^\dagger \sqrt{\rho_a} | j'\tau' m' \rangle \times \langle j'\tau' m' | \ln |\rho_b V_{\text{ani}} \sqrt{\rho_a} \mu - \rho_b \sqrt{\rho_a} \mu V_{\text{ani}} | j\tau m \ln \rangle, \quad (23)$$

where repeated indices $j, \tau, m, j', \tau', m', l$, and n mean a summation over them, and there is a range limitation with $E(j',\tau') < E(j,\tau)$ here. As shown by Eq. (23), many matrix elements of V_{ani} between states of a $\text{H}_2\text{O}-\text{N}_2$ pair are required, and the number is very large if most of the populated states are taken into account. Of course, to evaluate these matrix elements is possible, but it requires a lot of work unless V_{ani} has a very simple form. Usually one has to express V_{ani} in terms of an expansion of the product of $D_{mn}^{j''}(\alpha, \beta, \gamma)$ and $Y_{l''n''}(\theta, \varphi)$ first, where the angular arguments represent orientations of H_2O and N_2 , respectively. Then, one has to calculate matrix elements for each component and add the results obtained. In general, there are a lot of components in the expansion because the number of possible combination of $j'', m'', k'', l'',$ and n'' is large. Unfortunately, the evaluation of ${}_+\langle 1|\mathcal{L}_1|1\rangle_+$ does not help us too much. As shown later, one has to go further to calculate matrix elements of operators that contain powers of \mathcal{L}_1 . This implies that quantities like V_{ani}^2 appear in the calculations. If

one follows the usual procedure mentioned above, the calculation is intractable. This is one reason why, even for such an important problem, there has been little progress.

Recently, we have made progress in solving the problem of convergence in far-wing line shape calculations. We explain the problem and our solution briefly here. In order to calculate converged results, one has to include most of the populated states in calculations. However, as more states are included, the size of the interaction potential matrix, which is an off-diagonal operator, increases very fast and rapidly exceeds the computer limitation to handle a diagonalization procedure.⁷ As a result, to obtain converged results was difficult, in practice. The breakthrough arose from the idea that instead of choosing the internal states as the basis set in Hilbert space, one can select the orientations of the pair of molecules as the basis set.⁷ By introducing this coordinate representation, interactions are diagonal. As a result, summations over states become multidimensional integrations over the continuous angular variables and as many states as desired can be included in the calculations. The convergence criterion is transformed to the feasibility of calculating these integrations. As demonstrated in our study,³ using the Monte Carlo method one is able to calculate up to 11-dimensional integrations required for the most complicated pair consisting of two asymmetric top molecules. The calculations of the α_n and β_n^2 in the Lanczos algorithm are perfect candidates to apply our new method. In fact, the main computational tasks here are to evaluate matrix elements. With the coordinate representation, the job is transformed to multidimensional integrations, and with the Monte Carlo method, the latter can be successfully carried out. In addition, no matter how complicated V_{ani} is and no matter how many powers of V_{ani} appear, to calculate matrix elements is simple because in the coordinate representation, the integrands are just ordinary functions. It is these two powerful tools that enable us to make progress.

We adopt the simplifying notation that Ω_ζ is used to represent the orientation of the molecule of interest. For N_2 , Ω_ζ corresponds to θ_ζ and φ_ζ ; for H_2O , it corresponds to α_ζ , β_ζ , and γ_ζ . Then, we can express the basis function $|\zeta\rangle$ representing a specified orientation of the pair labeled by ζ as

$$|\zeta\rangle = |\delta(\Omega_a - \Omega_{a\zeta}) \delta(\Omega_b - \Omega_{b\zeta})\rangle. \quad (24)$$

We note that these basis functions are eigenfunctions of V_{ani} ,

$$V_{\text{ani}}(r, \Omega_a, \Omega_b) |\zeta\rangle = V_{\text{ani}}(r, \Omega_{a\zeta}, \Omega_{b\zeta}) |\zeta\rangle, \quad (25)$$

where $V_{\text{ani}}(r, \Omega_{a\zeta}, \Omega_{b\zeta})$ are the eigenvalues and they are simply values of V_{ani} at positions of the pair specified by r , $\Omega_{a\zeta}$, and $\Omega_{b\zeta}$. For simplicity, $V_{\text{ani}}(r, \Omega_{a\zeta}, \Omega_{b\zeta})$ will be denoted as $V_{\text{ani}}(\zeta)$. In terms of this basis set, one is able to rewrite ${}_+\langle 1 | \mathcal{L}_1 | 1 \rangle_+$ as

$${}_+\langle 1 | \mathcal{L}_1 | 1 \rangle_+ = \frac{1}{M_+} \int \int |\langle \zeta | \sqrt{\rho_a \rho_b} \mu_+ | \eta \rangle|^2 \times [V_{\text{ani}}(\zeta) - V_{\text{ani}}(\eta)] d\Omega_\zeta d\Omega_\eta, \quad (26)$$

where $d\Omega_\zeta$ denotes the volume element and the subscript $+$ of μ_+ implies that its components lie in a subspace constructed by the positive resonance lines only. We note that in

the coordinate representation $\sqrt{\rho_a \rho_b}$ is off-diagonal but the dipole moment μ is diagonal. However, because the positive resonance components μ_+ and the negative ones μ_- are distinguished here, one has to treat μ_+ and μ_- as off-diagonal operators.

Because the pair has a rotational symmetry, the dimensionality of Eq. (26) can always be reduced by one. Therefore, ${}_+\langle 1 | \mathcal{L}_1 | 1 \rangle_+$ is a nine-dimensional integration whose integrand consists of two factors: $|\langle \zeta | \sqrt{\rho_a \rho_b} \mu_+ | \eta \rangle|^2$ and $[V_{\text{ani}}(\zeta) - V_{\text{ani}}(\eta)]$. The first factor is constructed from the density matrices for H_2O and N_2 :

$$\begin{aligned} |\langle \zeta | \sqrt{\rho_a \rho_b} \mu_+ | \eta \rangle|^2 \\ = |\langle \delta(\Omega_a - \Omega_{a\zeta}) | \sqrt{\rho_a} \mu_+ | \delta(\Omega_a - \Omega_{a\eta}) \rangle|^2 \\ \times |\langle \delta(\Omega_b - \Omega_{b\zeta}) | \sqrt{\rho_b} | \delta(\Omega_b - \Omega_{b\eta}) \rangle|^2. \end{aligned} \quad (27)$$

For the linear molecule N_2 , we have shown that^{7,8}

$$\begin{aligned} |\langle \delta(\Omega_b - \Omega_{b\zeta}) | \sqrt{\rho_b} | \delta(\Omega_b - \Omega_{b\eta}) \rangle|^2 \\ = \sum_L B_L P_L(\cos \Theta_{b(\zeta\eta)}), \end{aligned} \quad (28)$$

where $P_L(\cos \Theta_{b(\zeta\eta)})$ are Legendre polynomials with $L = 0, 1, 2, \dots$, and $\Theta_{b(\zeta\eta)}$ is the angle between $\Omega_{b\zeta}$ and $\Omega_{b\eta}$, viz.,

$$\cos \Theta_{b(\zeta\eta)} = \cos \theta_{b\zeta} \cos \theta_{b\eta} + \sin \theta_{b\zeta} \sin \theta_{b\eta} \cos(\varphi_{b\zeta} - \varphi_{b\eta}). \quad (29)$$

The coefficients B_L are given by

$$\begin{aligned} B_L = \frac{1}{16\pi^2 Q_b} \sum_{l'l'} (2l+1)(2l'+1) \\ \times \sqrt{g_{ll'}} e^{-\beta[E(l)+E(l')]/2} C^2(l'l', L, 000). \end{aligned} \quad (30)$$

It is obvious that the density matrix for N_2 is a one-dimensional distribution whose argument is the angle between the initial and final orientations of N_2 . The profile of the absolute square of the density matrix for N_2 calculated from Eqs. (28) and (30) has been discussed in our previous study⁷ and will not be repeated here. On the other hand, because H_2O is an asymmetric top molecule, one expects that $|\langle \delta(\Omega_a - \Omega_{a\zeta}) | \sqrt{\rho_a} \mu_+ | \delta(\Omega_a - \Omega_{a\eta}) \rangle|^2$ is a three-dimensional distribution whose arguments are three Euler angles representing rotations between the initial and final orientations of H_2O .

As shown in our previous study,³ if one uses a high cutoff such as $J_{\text{max}} = 26$, to calculate this distribution requires a lot of CPU time, but is still feasible. However, if the interaction potential model used for the calculations in Eq. (26) contains cyclic coordinates, the three-dimensional distributions are reduced to an “averaged” one-dimensional distribution that can be obtained more easily and, in addition, the nine-dimensional integrations in Eq. (26) are reduced to seven-dimensional ones.⁸ As a result, one is able to reduce the difficulty of calculating matrix elements dramatically. Given the fact that there are several other matrix elements required, to limit CPU time we will assume that the potential model for $V_{\text{ani}}(r, \Omega_a, \Omega_b)$ contains cyclic coordinates. This assumption can be justified by the following argument. First

of all, the leading long-range dipole–quadrupole interaction of $\text{H}_2\text{O}-\text{N}_2$ has rotational symmetry about the Z axis of H_2O because in the II' representation, the dipole moment is along this direction. This term dominates other higher-order terms since the H_2O molecule has a large dipole moment. Therefore, the long-range part of $V_{\text{ani}}(r, \mathbf{\Omega}_a, \mathbf{\Omega}_b)$ is approximately independent of the Euler angle γ of H_2O . Second, as shown later, it is the long-range part not the short-range part of $V_{\text{ani}}(r, \mathbf{\Omega}_a, \mathbf{\Omega}_b)$ that plays a crucial role in the millimeter wave continuum absorption. Therefore, one can conclude that this assumption about $V_{\text{ani}}(r, \mathbf{\Omega}_a, \mathbf{\Omega}_b)$ is a good approximation in the present calculations. One can thus perform a two-dimensional integration over $\gamma_{a\zeta}$ and $\gamma_{a\eta}$ first. In fact, the procedure involves the density matrix $|\langle \delta(\mathbf{\Omega}_a - \mathbf{\Omega}_{a\zeta}) | \sqrt{\rho_a} \boldsymbol{\mu}_+ | \delta(\mathbf{\Omega}_a - \mathbf{\Omega}_{a\eta}) \rangle|^2$ only. It turns out that by using the fact that

$$\int_0^{2\pi} D_{mk}^j(\alpha, \beta, \gamma) d\gamma = 2\pi \delta_{k0} D_{m0}^j(\alpha, \beta), \quad (31)$$

where δ_{k0} is the Kronecker symbol, one is able to carry out this integration analytically and obtain

$$\begin{aligned} & \int_0^{2\pi} \int_0^{2\pi} |\langle \delta(\mathbf{\Omega}_a - \mathbf{\Omega}_{a\zeta}) | \sqrt{\rho_a} \boldsymbol{\mu}_+ | \delta(\mathbf{\Omega}_a - \mathbf{\Omega}_{a\eta}) \rangle|^2 d\gamma_{a\zeta} d\gamma_{a\eta} \\ &= \sum_L A_L P_L(\cos \Theta_{a(\zeta\eta)}), \end{aligned} \quad (32)$$

where $L=0,1,2,\dots$, and $\Theta_{a(\zeta\eta)}$ is the angle between the initial and final directions of the Z axis of a body-fixed frame for H_2O ; this expression is similar to that for N_2 given in Eq. (28). The coefficients A_L introduced in the above expression are defined by

$$\begin{aligned} A_L = & \frac{1}{16\pi^2 Q_a} (-1)^{1+L} \sum_{j_1 \tau_1} \sum_{j_2 \tau_2} \sum_{\{j'_1 \tau'_1\}_+} \sum_{\{j'_2 \tau'_2\}_+} (-1)^{j_1+j_2} \\ & \times (2j_1+1)(2j_2+1) \sqrt{(2j'_1+1)(2j'_2+1)} \\ & \times \sqrt{g_{\tau_1} g_{\tau_2}} e^{-\beta[E(j_1, \tau_1) + E(j_2, \tau_2)]/2} \\ & \times W(j'_2 j_2 j'_1 j_1, 1L) \boldsymbol{\mu}_{j_1 \tau_1; j'_1 \tau'_1} \boldsymbol{\mu}_{j_2 \tau_2; j'_2 \tau'_2} \\ & \times \left\{ \sum_k (-1)^k U_{k\tau_1}^{j_1} U_{k\tau_2}^{j_2} C(j_1 j_2 L, k-k_0) \right\} \\ & \times \left\{ \sum_{k'} (-1)^{k'} U_{k' \tau'_1}^{j'_1} U_{k' \tau'_2}^{j'_2} C(j'_1 j'_2 L, k'-k'_0) \right\}, \end{aligned} \quad (33)$$

where $W(j'_2 j_2 j'_1 j_1, 1L)$ is a Racah coefficient, and $\{j'_1 \tau'_1\}_+$ and $\{j'_2 \tau'_2\}_+$ indicate the summations over j'_1, τ'_1 and j'_2, τ'_2 are limited to $E(j'_1, \tau'_1) < E(j_1, \tau_1)$ and $E(j'_2, \tau'_2) < E(j_2, \tau_2)$, respectively. By comparing Eqs. (33) and (30), it is obvious that the expression for A_L associated with the “averaged” density matrix of H_2O is more complicated than B_L for N_2 . Fortunately, there are not too many A_L to evaluate. In fact, if one chooses $J_{\text{max}}=26$, the number of A_L is 53. However, before we carry out numerical calculations for the “averaged” density matrix of H_2O , we can first draw a conclusion about $+\langle 1 | \mathcal{L}_1 | 1 \rangle_+$. Because the integrand in Eq. (26) is antisymmetric with respect to ζ and η , the value of

$+\langle 1 | \mathcal{L}_1 | 1 \rangle_+$ is zero. Combining this fact with those derived in the last section, we can conclude that in order to calculate the millimeter wave continuum absorption for $\text{H}_2\text{O}-\text{N}_2$, one must consider a higher-order cutoff for the continued fraction because there are no contributions from the simplest approximation $(\omega - \alpha_1)^{-1}$.

E. Matrix elements of \mathcal{L}^n

As mentioned before, one big advantage resulting from the coordinate representation is that derivations of expressions for matrix elements involving powers of \mathcal{L}_1^n with $n > 1$ do not cause much more difficulty than for $+\langle 1 | \mathcal{L}_1 | 1 \rangle_+$. First of all, let us consider the matrix element $+\langle 1 | \mathcal{L}^2 | 1 \rangle_+$ which consists of four terms:

$$\begin{aligned} +\langle 1 | \mathcal{L}^2 | 1 \rangle_+ = & +\langle 1 | \mathcal{L}_a^2 | 1 \rangle_+ + \langle 1 | \mathcal{L}_1 \mathcal{L}_a | 1 \rangle_+ \\ & + \langle 1 | \mathcal{L}_a \mathcal{L}_1 | 1 \rangle_+ + \langle 1 | \mathcal{L}_1^2 | 1 \rangle_+. \end{aligned} \quad (34)$$

The first term is already known. In the following, unless necessary for clarity, we will adopt a convention that repeated integration variables imply integrations over them and we will omit the integration symbol. The second term can be expressed as

$$\begin{aligned} +\langle 1 | \mathcal{L}_1 \mathcal{L}_a | 1 \rangle_+ = & \frac{1}{M_+} \langle \eta | \boldsymbol{\mu}_+^\dagger \sqrt{\rho_a \rho_b} | \zeta \rangle \langle \zeta | \mathcal{L}_a \sqrt{\rho_a \rho_b} \boldsymbol{\mu}_+ | \eta \rangle \\ & \times [V_{\text{ani}}(\zeta) - V_{\text{ani}}(\eta)], \end{aligned} \quad (35)$$

which is very similar to that for $+\langle 1 | \mathcal{L}_1 | 1 \rangle_+$, except there is an extra Liouville operator \mathcal{L}_a appearing in the density matrix of H_2O . With the same procedure as before, we can carry out integrations of $\langle \delta(\mathbf{\Omega}_a - \mathbf{\Omega}_{a\eta}) | \boldsymbol{\mu}_+^\dagger \sqrt{\rho_a} | \delta(\mathbf{\Omega}_a - \mathbf{\Omega}_{a\zeta}) \rangle \langle \delta(\mathbf{\Omega}_a - \mathbf{\Omega}_{a\zeta}) | \mathcal{L}_a \sqrt{\rho_a} \boldsymbol{\mu}_+ | \delta(\mathbf{\Omega}_a - \mathbf{\Omega}_{a\eta}) \rangle$ over $\gamma_{a\zeta}$ and $\gamma_{a\eta}$ first and introduce the corresponding “averaged” density matrix of H_2O . It turns out that the latter is another one-dimensional distribution whose argument is $\Theta_{a(\zeta\eta)}$. Hence, we do not need to go further and can simply conclude that $+\langle 1 | \mathcal{L}_1 \mathcal{L}_a | 1 \rangle_+ = 0$. Similarly, we can conclude that $+\langle 1 | \mathcal{L}_a \mathcal{L}_1 | 1 \rangle_+ = 0$ also. Therefore, there is only one new nonzero term $+\langle 1 | \mathcal{L}_1^2 | 1 \rangle_+$ in $+\langle 1 | \mathcal{L}^2 | 1 \rangle_+$. One can easily write down the expression for $+\langle 1 | \mathcal{L}_1^2 | 1 \rangle_+$ without any more algebraic work. In fact, the expression for $+\langle 1 | \mathcal{L}_1^2 | 1 \rangle_+$ is the same as that for $+\langle 1 | \mathcal{L}_1 | 1 \rangle_+$ given by Eq. (26), except for a replacement of $[V_{\text{ani}}(\zeta) - V_{\text{ani}}(\eta)]$ by $[V_{\text{ani}}(\zeta) - V_{\text{ani}}(\eta)]^2$:

$$+\langle 1 | \mathcal{L}_1^2 | 1 \rangle_+ = \frac{1}{M_+} |\langle \zeta | \sqrt{\rho_a \rho_b} \boldsymbol{\mu}_+ | \eta \rangle|^2 [V_{\text{ani}}(\zeta) - V_{\text{ani}}(\eta)]^2. \quad (36)$$

The values of $+\langle 1 | \mathcal{L}_1^2 | 1 \rangle_+$ can be evaluated in two steps. First, we calculate the density matrix of N_2 at $T=296$ K and the “averaged” density matrix of H_2O at $T=296$ K from Eqs. (28) and (32), respectively. The results for the former, which has been mentioned in Sec. II D, are presented in Fig. 1 and the latter in Fig. 2 together with the corresponding results associated with $|1\rangle_-$. Using the Monte Carlo method, we carry out the seven-dimensional integrations in which the integrand is $[V_{\text{ani}}(\zeta) - V_{\text{ani}}(\eta)]^2$ and the product of the two distributions is the weighting function. Because V_{ani} is a function of r , the value of the seven-dimensional integrations

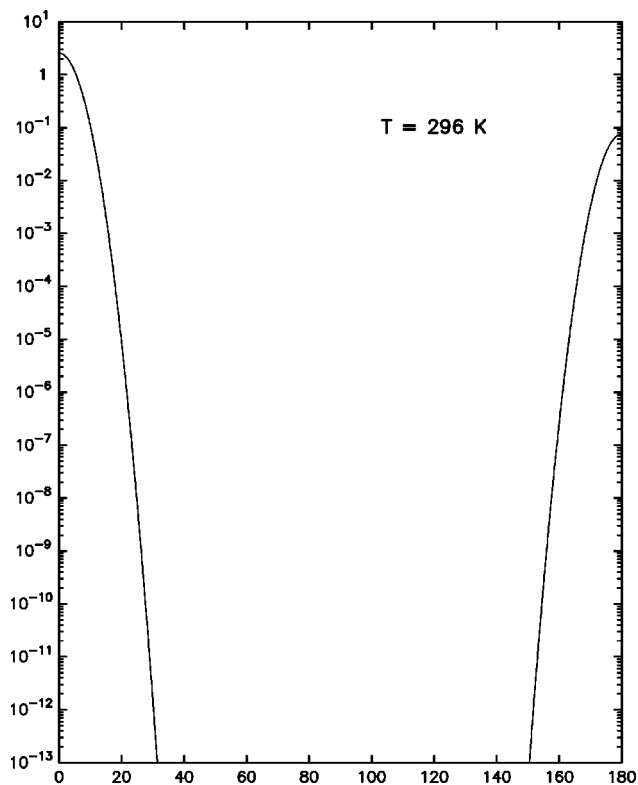


FIG. 1. The absolute square of the density matrix of N_2 given in the coordinate representation calculated at $T=296$ K for $J_{\max}=80$.

depends on r too. In practice, we select 80 values of r that span the interaction range and calculate the corresponding ${}_+\langle 1|\mathcal{L}_1^2|1\rangle_+$ for each specified r . In order to make sure that results obtained are reliable, we calculate a normalization constant of the weighting function simultaneously by setting the integrand equal to 1. The constant should be close to $16\pi^2 A_{L=0}$. Otherwise, it indicates that the matrix elements are not reliable. This procedure is carried out for all integrations. In general, all the calculations take several hours of CPU on a workstation. A detailed discussion about how to apply the Monte Carlo method to perform multidimensional integrations whose weighting functions have similar patterns as those in the present study has been reported previously,³ and we do not repeat it here.

Now let us consider the matrix element of ${}_+\langle 1|\mathcal{L}^3|1\rangle_+$ which contains eight terms. According to the powers of \mathcal{L}_1 , the latter are catalogued into four groups:

$$\begin{aligned} {}_+\langle 1|\mathcal{L}^3|1\rangle_+ &= {}_+\langle 1|\mathcal{L}_a^3|1\rangle_+ \\ &+ {}_+\langle 1|\mathcal{L}_1\mathcal{L}_a^2+\mathcal{L}_a^2\mathcal{L}_1+\mathcal{L}_a\mathcal{L}_1\mathcal{L}_a|1\rangle_+ \\ &+ {}_+\langle 1|\mathcal{L}_1^2\mathcal{L}_a+\mathcal{L}_a\mathcal{L}_1^2+\mathcal{L}_1\mathcal{L}_a\mathcal{L}_1|1\rangle_+ \\ &+ {}_+\langle 1|\mathcal{L}_1^3|1\rangle_+. \end{aligned} \quad (37)$$

Among them, only the third group needs to be evaluated because the first one ${}_+\langle 1|\mathcal{L}_a^3|1\rangle_+$ is already known and, similar to ${}_+\langle 1|\mathcal{L}_1\mathcal{L}_a+\mathcal{L}_a\mathcal{L}_1|1\rangle_+$, we can conclude that the second and the fourth groups are zero. With respect to the third, we have to calculate ${}_+\langle 1|\mathcal{L}_1^2\mathcal{L}_a+\mathcal{L}_a\mathcal{L}_1^2|1\rangle_+$ and ${}_+\langle 1|\mathcal{L}_1\mathcal{L}_a\mathcal{L}_1|1\rangle_+$ separately. The former can be expressed as

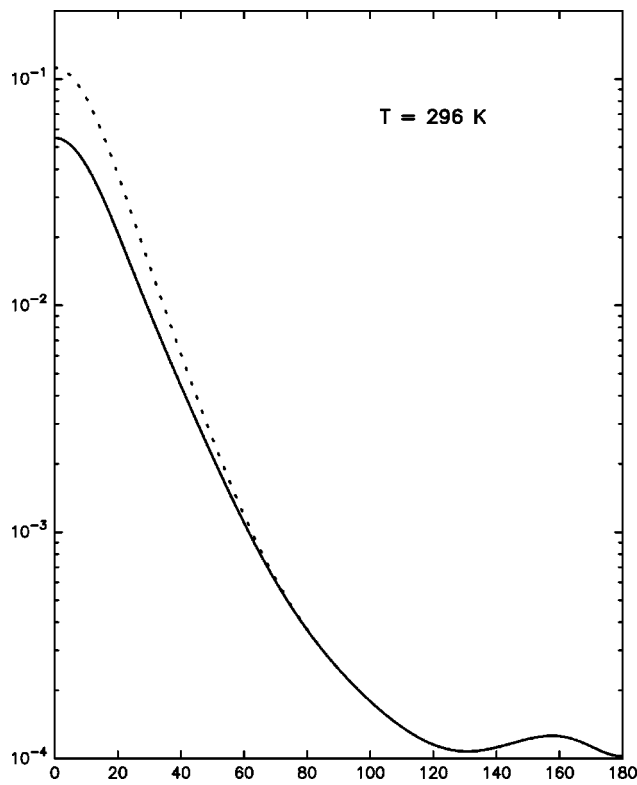


FIG. 2. The one-dimensional distributions of the density matrix of H_2O at $T=296$ K for $J_{\max}=26$. The solid and dotted lines are associated with $|1\rangle_+$ and $|1\rangle_-$, respectively.

$$\begin{aligned} &{}_+\langle 1|\mathcal{L}_1^2\mathcal{L}_a+\mathcal{L}_a\mathcal{L}_1^2|1\rangle_+ \\ &= \frac{1}{M_+} \{ \langle \eta | \boldsymbol{\mu}_+^\dagger \sqrt{\rho_a \rho_b} | \xi \rangle \langle \xi | \mathcal{L}_a \sqrt{\rho_a \rho_b} \boldsymbol{\mu}_+ | \eta \rangle \\ &\quad + \langle \eta | (\mathcal{L}_a \sqrt{\rho_a \rho_b} \boldsymbol{\mu}_+)^\dagger | \xi \rangle \langle \xi | \sqrt{\rho_a \rho_b} \boldsymbol{\mu}_+ | \eta \rangle \} \\ &\quad \times [V_{\text{ani}}(\xi) - V_{\text{ani}}(\eta)]^2. \end{aligned} \quad (38)$$

Analogous to Eq. (36), ${}_+\langle 1|\mathcal{L}_1^2\mathcal{L}_a+\mathcal{L}_a\mathcal{L}_1^2|1\rangle_+$ is a seven-dimensional integration of $[V_{\text{ani}}(\xi) - V_{\text{ani}}(\eta)]^2$, with the first factor in Eq. (38) serving as the weighting function. This is a product of two distributions: the first associated with N_2 is the same as before, and the one associated with H_2O has to be calculated. It is easy to show that the latter can be expressed by formulas similar to those derived previously for $\langle \eta | \boldsymbol{\mu}_+^\dagger \sqrt{\rho_a} | \xi \rangle \langle \xi | \sqrt{\rho_a} \boldsymbol{\mu}_+ | \eta \rangle (= |\langle \xi | \sqrt{\rho_a} \boldsymbol{\mu}_+ | \eta \rangle|^2)$ shown by Eqs. (32) and (33). The only difference is that it comes from a new set of coefficients A_L whose expression is almost the same as Eq. (33), except that an extra factor $[E(j_1, \tau_1) - E(j'_1, \tau'_1)] + [E(j_2, \tau_2) - E(j'_2, \tau'_2)]$ is inserted inside the summation loops over the indices $j_1, \tau_1, j'_1, \tau'_1, j_2, \tau_2, j'_2, \tau'_2$. The distributions associated with ${}_+\langle 1|\mathcal{L}_1^2\mathcal{L}_a+\mathcal{L}_a\mathcal{L}_1^2|1\rangle_+$ and ${}_-\langle 1|\mathcal{L}_1^2\mathcal{L}_a+\mathcal{L}_a\mathcal{L}_1^2|1\rangle_-$ are presented in Fig. 3. Finally, we note that the CPU time for calculating ${}_+\langle 1|\mathcal{L}_1^2\mathcal{L}_a+\mathcal{L}_a\mathcal{L}_1^2|1\rangle_+$ is the same as for ${}_+\langle 1|\mathcal{L}_1^2|1\rangle_+$.

Now, we focus our attention on ${}_+\langle 1|\mathcal{L}_1\mathcal{L}_a\mathcal{L}_1|1\rangle_+$ whose explicit expression requires more algebraic work because the two \mathcal{L}_1 are separated by one \mathcal{L}_a here. One can write ${}_+\langle 1|\mathcal{L}_1\mathcal{L}_a\mathcal{L}_1|1\rangle_+$ as a summation of three terms:

$$\begin{aligned}
+ \langle 1 | \mathcal{L}_1 \mathcal{L}_a \mathcal{L}_1 | 1 \rangle_+ &= - \frac{1}{M_+} \{ \langle \eta | \mu_+^\dagger \sqrt{\rho_a \rho_b} | \zeta \rangle \langle \zeta | \mathcal{L}_a \sqrt{\rho_a \rho_b} \mu_+ | \eta \rangle + \langle \eta | (\mathcal{L}_a \sqrt{\rho_a \rho_b} \mu_+)^{\dagger} | \zeta \rangle \langle \zeta | \sqrt{\rho_a \rho_b} \mu_+ | \eta \rangle \} V_{\text{ani}}(\zeta) V_{\text{ani}}(\eta) \\
&+ \frac{1}{M_+} \langle \eta | \rho_b \mu_+^\dagger H_a \rho_a \mu_+ - \rho_b \sqrt{\rho_a} \mu_+ H_a \mu_+^\dagger \sqrt{\rho_a} | \eta \rangle V_{\text{ani}}(\eta)^2 \\
&+ \frac{1}{M_+} \langle \eta | \rho_b \sqrt{\rho_a} \mu_+^\dagger \sqrt{\rho_a} - \rho_b \mu_+^\dagger \rho_a \mu_+ | \zeta \rangle \langle \zeta | H_a | \eta \rangle V_{\text{ani}}(\zeta) V_{\text{ani}}(\eta), \quad (39)
\end{aligned}$$

and all of them are multidimensional integrations. By comparing the first term with Eq. (38), it is clear that its expression is almost the same as that for $+\langle 1 | \mathcal{L}_1^2 \mathcal{L}_a + \mathcal{L}_a \mathcal{L}_1^2 | 1 \rangle_+$, except that the integrand becomes $V_{\text{ani}}(\zeta) V_{\text{ani}}(\eta)$. By using the same weighting function derived for $+\langle 1 | \mathcal{L}_1^2 \mathcal{L}_a + \mathcal{L}_a \mathcal{L}_1^2 | 1 \rangle_+$, one can carry out the seven-dimensional integrations of $V_{\text{ani}}(\zeta) V_{\text{ani}}(\eta)$ and obtain values for this term.

With respect to the second term of Eq. (39), it is given in terms of four-dimensional integrations of $V_{\text{ani}}(\eta)^2$ over η with an associated weighting function. As before, this weighting function is a product of two factors: one associated with N_2 and one with H_2O . The former is given by $\langle \delta(\mathbf{\Omega}_b - \mathbf{\Omega}_{b\eta}) | \rho_b | \delta(\mathbf{\Omega}_b - \mathbf{\Omega}_{b\eta}) \rangle$ and is simply the constant $1/4\pi$. With some algebraic work, one can show that the latter is $+\langle v | \mathcal{L}_a | v \rangle_+ / 4\pi$, which is known. Then, the weighting function becomes $+\langle v | \mathcal{L}_a | v \rangle_+ / 16\pi^2$ and is independent of

η . As a result, we can conclude that the second term in Eq. (39) is given by

$$\begin{aligned}
&\frac{1}{M_+} \langle \eta | \rho_b \mu_+^\dagger H_a \rho_a \mu_+ - \rho_b \sqrt{\rho_a} \mu_+ H_a \mu_+^\dagger \sqrt{\rho_a} | \eta \rangle V_{\text{ani}}(\eta)^2 \\
&= + \langle 1 | \mathcal{L}_a | 1 \rangle_+ \overline{V_{\text{ani}}^2}, \quad (40)
\end{aligned}$$

where the notation $\overline{V_{\text{ani}}^2}$ is introduced to represent an average of $V_{\text{ani}}(\eta)^2$ over η . Of course, $\overline{V_{\text{ani}}^2}$ is a function of r .

Similarly, the third term is given in terms of integrations of $V_{\text{ani}}(\zeta) V_{\text{ani}}(\eta)$ over ζ and η with a different weighting function, which is a product of two distributions. Using the well-known formula

$$\frac{1}{4\pi} \sum_{L=0}^{\infty} (2L+1) P_L(x) = \delta(x), \quad (41)$$

it is easy to show that the distribution associated with N_2 becomes a Dirac delta function $\delta(\mathbf{\Omega}_{b\zeta} - \mathbf{\Omega}_{b\eta})$ when the number of states of N_2 included goes to infinity. This enables us to carry out part of the integration analytically and reduce the dimensionality of the remaining one by 2. On the other hand, there is no difficulty to derive the distribution for H_2O that is plotted in Fig. 4 together with its partner derived for $|1\rangle_-$. As shown in the figure, the distributions oscillate wildly and, in fact, the numbers of oscillations are equal to $J_{\text{max}}/2$. Therefore, one must be careful in these calculations because this kind of behavior could cause big errors when one evaluates the integrations of $V_{\text{ani}}(\xi) V_{\text{ani}}(\eta)$. In order to make sure that the results obtained are reliable, we use an alternative way to carry out the calculation. We introduce a reasonable approximation for $V_{\text{ani}} H_a V_{\text{ani}}$ by ignoring the higher-order commutator term,

$$\begin{aligned}
V_{\text{ani}} H_a V_{\text{ani}} &= (V_{\text{ani}}^2 H_a + H_a V_{\text{ani}}^2) / 2 + [V_{\text{ani}}, [H_a, V_{\text{ani}}]] \\
&\approx (V_{\text{ani}}^2 H_a + H_a V_{\text{ani}}^2) / 2. \quad (42)
\end{aligned}$$

Then, one is able to show that the approximate third term is equal to $+\langle 1 | \mathcal{L}_a | 1 \rangle_+ \overline{V_{\text{ani}}^2}$. Numerical tests show that differences between these two results are less than 1%. Thus, we can conclude that we can calculate $+\langle 1 | \mathcal{L}_1 \mathcal{L}_a \mathcal{L}_1 | 1 \rangle_+$ accurately. We note that by comparing the values of $+\langle 1 | \mathcal{L}_1 \mathcal{L}_a \mathcal{L}_1 | 1 \rangle_+$ with those of $+\langle 1 | \mathcal{L}_1^2 \mathcal{L}_a + \mathcal{L}_a \mathcal{L}_1^2 | 1 \rangle_+$, it seems that the former is about half of the latter. This observation will be used later.

We will not present detailed discussions for $+\langle 1 | \mathcal{L}^4 | 1 \rangle_+$, which consists of 16 terms. Among them, we already know the value of $+\langle 1 | \mathcal{L}_a^4 | 1 \rangle_+$, and four other terms containing one \mathcal{L}_1 operator are zero. With respect to six terms containing two \mathcal{L}_1 operators, we group them into two groups: $+\langle 1 | \mathcal{L}_a^2 \mathcal{L}_1^2 + \mathcal{L}_1^2 \mathcal{L}_a^2 + \mathcal{L}_a \mathcal{L}_1^2 \mathcal{L}_a | 1 \rangle_+$ and

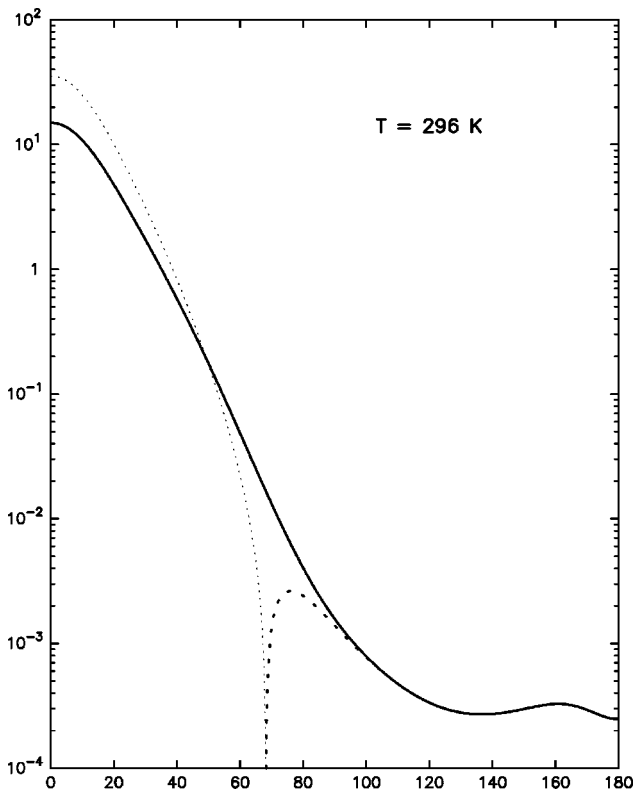


FIG. 3. The one-dimensional distributions of H_2O obtained at $T = 296 \text{ K}$ for $J_{\text{max}} = 26$, which are the weighting functions used to evaluate the matrix elements $+\langle 1 | \mathcal{L}_1^2 \mathcal{L}_a + \mathcal{L}_a \mathcal{L}_1^2 | 1 \rangle_+$ and $-\langle 1 | \mathcal{L}_1^2 \mathcal{L}_a + \mathcal{L}_a \mathcal{L}_1^2 | 1 \rangle_-$ and are represented by the solid and dotted curves, respectively. Because the values of the latter are negative at small angles, we use a thin line to plot its absolute magnitude.

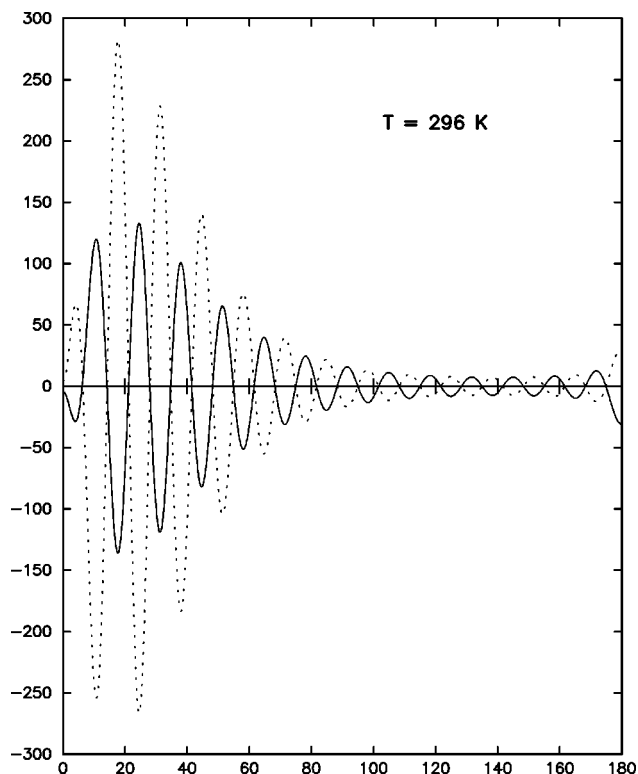


FIG. 4. The one-dimensional distributions of H₂O obtained at $T = 296$ K for $J_{\max} = 26$, which are used to evaluate parts of the matrix elements ${}_+\langle 1 | \mathcal{L}_1 \mathcal{L}_a \mathcal{L}_1 | 1 \rangle_+$ and ${}_-\langle 1 | \mathcal{L}_1 \mathcal{L}_a \mathcal{L}_1 | 1 \rangle_-$, respectively. The former (the solid line) is derived from the third term of Eq. (39). The latter (the dotted line) is its partner. As shown in the figure, each of them oscillates 13 ($=J_{\max}/2$) times.

${}_+\langle 1 | \mathcal{L}_a \mathcal{L}_1 \mathcal{L}_a \mathcal{L}_1 + \mathcal{L}_1 \mathcal{L}_a \mathcal{L}_1 \mathcal{L}_a + \mathcal{L}_1 \mathcal{L}_a^2 \mathcal{L}_1 | 1 \rangle_+$. For the former, using the same method as that used in calculating ${}_+\langle 1 | \mathcal{L}_1^2 \mathcal{L}_a + \mathcal{L}_a \mathcal{L}_1^2 | 1 \rangle_+$, we are able to obtain the values. For the latter, as expected, problems similar to what happened in ${}_+\langle 1 | \mathcal{L}_1 \mathcal{L}_a \mathcal{L}_1 | 1 \rangle_+$ occur, but the situation becomes even worse. The most severe trouble results from the operator $\mathcal{L}_1 \mathcal{L}_a^2 \mathcal{L}_1$, where two \mathcal{L}_1 are separated by \mathcal{L}_a^2 . The corresponding weighting function oscillates so wildly that one is not able to obtain reliable integration values at all. In the present study, we simply estimate ${}_+\langle 1 | \mathcal{L}_1 \mathcal{L}_a^2 \mathcal{L}_1 | 1 \rangle_+$ by using the observation found above. We assume that the values of ${}_+\langle 1 | \mathcal{L}_1 \mathcal{L}_a^2 \mathcal{L}_1 | 1 \rangle_+$ are equal to half of ${}_+\langle 1 | \mathcal{L}_a \mathcal{L}_1 \mathcal{L}_a \mathcal{L}_1 + \mathcal{L}_1 \mathcal{L}_a \mathcal{L}_1 \mathcal{L}_a | 1 \rangle_+$ because the former contains one term and the latter contains two terms. Concerning the remaining five terms associated with $\mathcal{L}_a \mathcal{L}_1^3$, $\mathcal{L}_1^3 \mathcal{L}_a$, $\mathcal{L}_1 \mathcal{L}_a \mathcal{L}_1^2$, $\mathcal{L}_1^2 \mathcal{L}_a \mathcal{L}_1$, and \mathcal{L}_1^4 , the first two are zero, and we will ignore the others because for case of interest here $\mathcal{L}_1 < \mathcal{L}_a$ and, in comparison with those terms that have been taken into account, these terms are higher-order corrections.

Similarly, there are 32 terms in ${}_+\langle 1 | \mathcal{L}_a^5 | 1 \rangle_+$. We already know ${}_+\langle 1 | \mathcal{L}_a^5 | 1 \rangle_+$ and five zero terms containing one \mathcal{L}_1 . Again, we group ten terms containing two \mathcal{L}_1 operators into two categories: ${}_+\langle 1 | \mathcal{L}_a^3 \mathcal{L}_1^2 + \mathcal{L}_1^2 \mathcal{L}_a^3 + \mathcal{L}_a^2 \mathcal{L}_1^2 \mathcal{L}_a + \mathcal{L}_a \mathcal{L}_1^2 \mathcal{L}_a^2 | 1 \rangle_+$ and ${}_+\langle 1 | \mathcal{L}_a \mathcal{L}_1 \mathcal{L}_a \mathcal{L}_1 \mathcal{L}_a + \mathcal{L}_a^2 \mathcal{L}_1 \mathcal{L}_a \mathcal{L}_1 + \mathcal{L}_1 \mathcal{L}_a \mathcal{L}_1 \mathcal{L}_a^2 + \mathcal{L}_1 \mathcal{L}_a^2 \mathcal{L}_1 \mathcal{L}_a + \mathcal{L}_a \mathcal{L}_1 \mathcal{L}_a^2 \mathcal{L}_1 + \mathcal{L}_1 \mathcal{L}_a^3 \mathcal{L}_1 | 1 \rangle_+$. We calculate the first group. With respect to the second group, we calculate the first three terms and estimate the remaining

ones by assuming that they equal the former. We will also ignore the remaining higher-order correction terms in ${}_+\langle 1 | \mathcal{L}_a^5 | 1 \rangle_+$. Therefore, all matrix elements required are available and there are no more calculations involving the internal degrees of freedom.

F. Poles and residues of the fractions

After all the matrix elements of ${}_+\langle 1 | \mathcal{L}^n | 1 \rangle_+$ up to $n = 5$ are known, one can easily calculate α_1 , β_2^2 , α_2 , β_3^2 , and α_3 . We find that α_1 is a constant (95.1928 cm^{-1}) because ${}_+\langle 1 | \mathcal{L} | 1 \rangle_+ = {}_+\langle 1 | \mathcal{L}_a | 1 \rangle_+$ and all the others are smooth functions of r and approach their asymptotic values (i.e., as r goes to infinity) derived previously without considering the interaction, but we do not present their plots here. In addition, one can verify that the convergence criterion, Eq. (15), is satisfied. Then, in terms of these functions, the inner trace of $F(\omega)$ can be expressed as

$${}_+\left\langle 1 \left| \frac{1}{\omega - \mathcal{L}} \right| 1 \right\rangle_+ = \frac{1}{\omega - \alpha_1 - \frac{\beta_2^2}{\omega - \alpha_2 - \frac{\beta_3^2}{\omega - \alpha_3}}} = \sum_{i=1}^3 \frac{R_i}{\omega - z_i}. \quad (43)$$

The last step in Eq. (43) is based on a theorem about the poles and residues of the continued fraction.¹³ If α_1 , α_2 , and α_3 are real and β_2^2 and β_3^2 are positive, as is the case here, the fraction can be expressed in terms of its poles and residues, and these poles z_i are real and distinct and the residues R_i are positive. There is no difficulty in finding z_i because they are the roots of a cubic equation,

$$(\omega - \alpha_1)(\omega - \alpha_2)(\omega - \alpha_3) - (\omega - \alpha_1)\beta_3^2 - (\omega - \alpha_2)\beta_2^2 = 0, \quad (44)$$

and there are analytical expressions available. On the other hand, one can easily show that R_i are given by

$$R_i = \{(z_i - \alpha_2)(z_i - \alpha_3) - \beta_3^2\}(z_j - z_k) / \times \{z_1^2(z_2 - z_3) + z_2^2(z_3 - z_1) + z_3^2(z_1 - z_2)\}, \quad (45)$$

where the indices i, j , and k are in cyclic order. Finally, we note that because β_2^2 , α_2 , β_3^2 , and α_3 are functions of r , z_i , and R_i are functions of r too. In the present study, because we are interested in the millimeter wave spectral region, we will focus our attention on those poles that are within or close to this frequency region. We present the calculated poles of interest as functions of r for $T = 270, 296$, and 330 K in Fig. 5. For each temperature, there is a pair of curves associated with $|1\rangle_+$ and $|1\rangle_-$; the positive slope curve belongs to the former and the negative one to the latter. As shown in the figure, all of them are smooth curves and approach asymptotic limits as r goes to infinity. For example, the two curves for $T = 296$ K approach 46.1918 and -55.9511 cm^{-1} , respectively. However, the parts of curves of most interest are those whose values are within 0 – 15 cm^{-1} . In practice, we have to extend this region by a few cm^{-1} , such as -3 – 18 cm^{-1} because we need to evaluate some deriva-

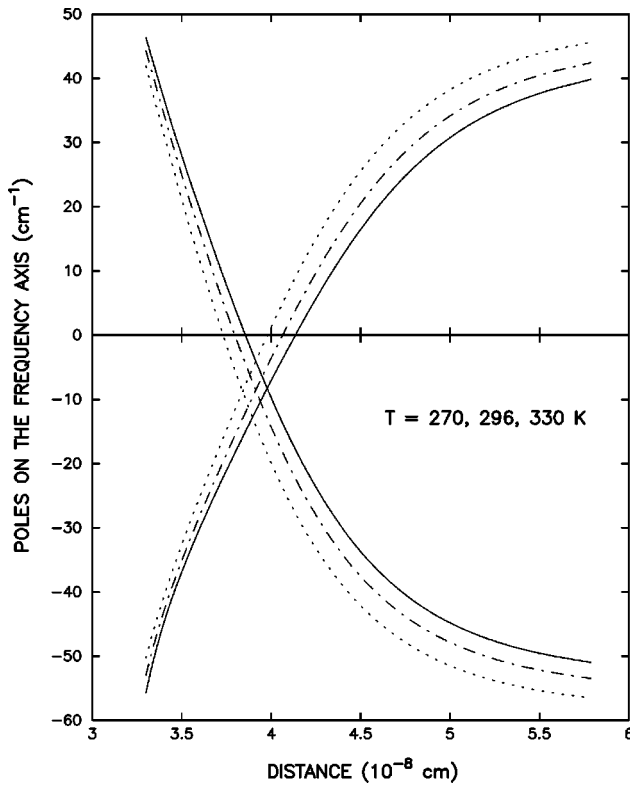


FIG. 5. The calculated poles of the continued fraction as functions of r for $T=270, 296$, and 330 K. They are represented by the solid, dot-dashed, and dotted lines, respectively. For a specified temperature, there are two set of curves associated with $|1\rangle_+$ and $|1\rangle_-$, respectively. Each set consists of three curves but only the one passing through the millimeter spectral region is presented. As r increases, the positive slope curve belongs to $|1\rangle_+$ and the negative one to $|1\rangle_-$.

tives. For $T=296$ K, this region is located at separations between 3.5 and 4.5 Å. By comparing curves representing different temperatures, we find that the separations of interest become smaller as the temperature increases. With respect to residues associated with the poles of interest, we find that they are also smooth functions of r , and their values are positive and less than 1, but we do not present them here.

G. A classical ensemble average over the translational motion

After all the poles and residues are known, we have completed the evaluation of the trace Tr_{ab} and can express the results as

$$\begin{aligned} \text{Tr}_{ab} & \left(\mu^\dagger \sqrt{\rho_a \rho_b} \frac{1}{\omega - \mathcal{L}} \sqrt{\rho_a \rho_b} \mu \right) \\ &= \mu^2 M_+ \sum_{i=1}^3 \frac{R_i^{(+)}(r)}{\omega - z_i^{(+)}(r)} + \mu^2 M_- \sum_{i=1}^3 \frac{R_i^{(-)}(r)}{\omega - z_i^{(-)}(r)}, \quad (46) \end{aligned}$$

where the superscripts (+) and (−) are attached to the poles and residues to distinguish their associations, and their dependencies on r are explicitly indicated. Now, we are ready to perform the remaining trace operator Tr_r in Eq. (8); i.e., an ensemble average over the translational motion of the molecules.

Because the millimeter wave spectral region is far away from the strong lines of the pure-rotational band of H_2O , we introduce the quasistatic approximation in which the collisions are assumed to be of infinite duration and the translational motions can be treated classically. Then, the ensemble average of results obtained from the trace Tr_{ab} over the translational motion becomes an integration over r from 0 to infinity with ρ_{iso} as its weighting function. From Eqs. (8) and (46), we are able to write the spectral density $F(\omega)$ as

$$\begin{aligned} F(\omega) &= 4\pi\mu^2 M_+ \sum_{i=1}^3 \int_0^\infty \delta[\omega - z_i^{(+)}(r)] e^{-\beta V_{\text{iso}}(r)} \\ & \quad \times R_i^{(+)}(r) r^2 dr + 4\pi\mu^2 M_- \\ & \quad \times \sum_{i=1}^3 \int_0^\infty \delta[\omega - z_i^{(-)}(r)] e^{-\beta V_{\text{iso}}(r)} R_i^{(-)}(r) r^2 dr, \quad (47) \end{aligned}$$

where we have used the the well-known formula

$$\lim_{\epsilon \rightarrow 0^+} \frac{1}{\omega + i\epsilon - z} = P \frac{1}{\omega - z} - i\pi \delta(\omega - z), \quad (48)$$

where P indicates the Cauchy principal value of the integral. We note that in order to include a statistical weight resulting from $V_{\text{ani}}(r)$, an extra factor $\rho_{\text{ani}}(r)$, defined by

$$\rho_{\text{ani}}(r) = \frac{1}{V} \int \int e^{-\beta V_{\text{ani}}(r, \Omega_a, \Omega_b)} d\Omega_a d\Omega_b, \quad (49)$$

where V is the volume of integration, should be inserted in Eq. (47). However, in the present study, because values of $\rho_{\text{ani}}(r)$ are very close to 1, the effect from including this factor is negligible.

It may appear that there is an another step required in Eq. (47) before one is able to evaluate values of $F(\omega)$. Usually, one needs to find roots for a specified frequency ω from the equations $z_i^{(+)}(r) - \omega = 0$ and $z_i^{(-)}(r) - \omega = 0$, with $i = 1, 2$, and 3 . In general, there is no problem to find these roots directly by solving the equations numerically after $z_i^{(+)}(r)$ and $z_i^{(-)}(r)$, as functions of r are known. However, this step is unnecessary. In fact, every selected r is a common root for six frequencies: $z_1^{(+)}(r)$, $z_2^{(+)}(r)$, $z_3^{(+)}(r)$, $z_1^{(-)}(r)$, $z_2^{(-)}(r)$, and $z_3^{(-)}(r)$. Therefore, instead of finding roots for any frequency of interest, one can simply screen two set of $z_i^{(+)}(r)$ and $z_i^{(-)}(r)$ and pick up those within the millimeter spectral region. For example, assume that $z_1^{(+)}(r_0)$ is one of them. With Eqs. (6) and (47), we can calculate the value of $F(\omega_0)$ with $\omega_0 = z_1^{(+)}(r_0)$ and obtain the corresponding contribution to the absorption coefficient at this frequency,

$$\begin{aligned} \alpha(\omega_0) &= \frac{16\pi^3}{3\hbar c} \beta \hbar n_{\text{pair}} \omega_0^2 \mu^2 M_+ \frac{R_1^{(+)}(r_0)}{|z_1'^{(+)}(r_0)|} \\ & \quad \times r_0^2 e^{-\beta V_{\text{iso}}(r_0)} \rho_{\text{ani}}(r_0), \quad (50) \end{aligned}$$

where the factor of $[\exp(\beta \hbar \omega_0) - 1]$ has been approximated by $\beta \hbar \omega_0$ and $z_1'^{(+)}(r) \equiv dz_1^{(+)}(r)/dr$. As shown by Eq. (50), the calculation of $\alpha(\omega_0)$ is straightforward because all quantities appearing on the right are known.

Numerical tests show that for the triplets $\{z_1^{(+)}(r), z_2^{(+)}(r), \text{ and } z_3^{(+)}(r)\}$, at most, there is only one of them located within the millimeter wave spectral region. The same conclusion is also true for $\{z_i^{(-)}(r), i=1, 2, \text{ and } 3\}$. This indicates that although the index i runs from 1 to 3, there is only one choice of $z_i^{(+)}(r)$ and $z_i^{(-)}(r)$ of interest and they are just those plotted in Fig. 5. Without loss of generality, we denote this choice as $i=1$. As shown in Fig. 5, these $z_1^{(+)}(r)$ and $z_1^{(-)}(r)$ are smooth functions of r and, in addition, they do not cross in the millimeter wave region. This implies that the two ranges of r that make contributions to $\alpha(\omega)$, one from $z_1^{(+)}(r)$ and one from $z_1^{(-)}(r)$, do not overlap.

Based on discussions given above, one can pursue the final calculations in the following way. With Eq. (50), we calculate all of $\alpha(z_1^{(+)}(r_0))$ with $z_1^{(+)}(r_0)$ located between, say, -3 to 18 cm^{-1} . In practice, we obtain a few dozen values, the exact number of which depends on the resolution of r used. Because all quantities appearing in Eq. (50) are smooth functions of r , these values vary smoothly as $z_1^{(+)} \times (r_0)$ varies. Then, for any frequency ω of interest, one can easily obtain $\alpha(\omega)$ using the interpolation method. Starting from an equation similar to Eq. (50), we repeat the same procedure for $z_1^{(-)}(r)$ and obtain another $\alpha(\omega)$. By adding these two, we obtain the final value of $\alpha(\omega)$.

H. Interaction potential

Before presenting numerical results for the millimeter wave continuum, we discuss briefly the interaction model used in the calculations. As mentioned previously, in order to facilitate the calculations, we assume that the interaction potential contains cyclic coordinates. Because in the present study the optimization of potential models and their parameters is not our main concern, we simply adopt the model for the $\text{H}_2\text{O}-\text{N}_2$ pair used in our previous work,⁸ which contains rotational symmetry about the Z axis of H_2O . The anisotropic part $V_{\text{ani}}(r, \mathbf{\Omega}_a, \mathbf{\Omega}_b)$ consists of a long-range dipole-quadrupole interaction, given by

$$V_{\text{dq}}(r, \mathbf{\Omega}_a, \mathbf{\Omega}_b) = \frac{3\mu\Theta}{2r^4} [\cos\beta_a(3\cos^2\theta_b - 1) - 2\sin\beta_a\sin\theta_b\cos\theta_b\cos(\alpha_a - \varphi_b)], \quad (51)$$

where Θ is the quadrupole moment of N_2 , and a short-range repulsive interaction represented by a site-site model,¹⁴

$$V_{\text{sr}}(r, \mathbf{\Omega}_a, \mathbf{\Omega}_b) = V_0 \sum_{i \in a} \sum_{j \in b} e^{-r_{ij}/\rho_0}, \quad (52)$$

where V_0 and ρ_0 are two parameters. The dipole moment of H_2O and the quadrupole moment of N_2 are well known and the values used in the present calculations are $\mu = 1.8546 \text{ D}$ and $\Phi = 1.466 \text{ D \AA}$, respectively.^{15,16} In the site-site model, the indices i and j run over force centers of the absorber a (i.e., H_2O) and the perturber b (i.e., N_2), respectively, and r_{ij} is the distance between the center i and the center j . The force centers of N_2 are located on the two N atoms, whose separation is 1.10 \AA , and the force centers of H_2O are located on its Z axis; their distances to the center of mass are equal to

0.07 and 0.56 \AA , respectively. Values of V_0 and ρ_0 are chosen as $V_0/k = 1.0 \times 10^7 \text{ K}$ and $\rho_0 = 0.22 \text{ \AA}$. We note that the profiles of the poles shown in Fig. 5 were obtained based on this anisotropic interaction model.

On the other hand, the isotropic interaction is represented by a Lennard-Jones model,

$$V_{\text{iso}}(r) = 4\epsilon \left[\left(\frac{\sigma}{r} \right)^{12} - \left(\frac{\sigma}{r} \right)^6 \right], \quad (53)$$

where ϵ and σ are the parameters. We note that $V_{\text{ani}}(r, \mathbf{\Omega}_a, \mathbf{\Omega}_b)$ is the most crucial factor in the whole calculation process, whereas $V_{\text{iso}}(r)$ does not play any role until the last step in which the average over the translation motion is carried out. As a result, to adjust the model of $V_{\text{ani}}(r, \mathbf{\Omega}_a, \mathbf{\Omega}_b)$ and its parameters requires the bulk of CPU time (about one day on one workstation) because one has to start each time from the very beginning. Meanwhile, to adjust $V_{\text{iso}}(r)$ is easy and one can get results in a few seconds. By comparing results obtained from different choices of the Lennard-Jones parameters, we adopt the values of $\epsilon = 3.31 \text{ \AA}$ and $\sigma/k = 155 \text{ K}$. Based on a combination of the corresponding $V_{\text{iso}}(r)$ and the $V_{\text{ani}}(r, \mathbf{\Omega}_a, \mathbf{\Omega}_b)$ mentioned previously, theoretical predictions of the second virial coefficients (i.e., $B_T = 34.43, 27.69, 22.10, \text{ and } 17.42 \text{ cm}^3/\text{mol}$ for $T = 298.15, 323.15, 348.15, \text{ and } 373.15 \text{ K}$, respectively) agree well with measurements (i.e., $B_T = 40 \pm 6, 28 \pm 5, 20 \pm 4, 15.5 \pm 3 \text{ cm}^3/\text{mol}$, accordingly).¹⁷

I. Numerical results

In our calculations, we first select 80 values of separation r to cover the whole range of the interaction and roughly calculate the corresponding values of the matrix elements. Based on these results, we derive the poles of the continued fractions and find those separations within $3.0\text{--}5.7 \text{ \AA}$ that pertain to the poles located in the millimeter wave spectral region. We then reselect another 80 points within a narrower interval. Again, by using more random evaluations in the Monte Carlo method, we derive the corresponding 80 values for each of the matrix elements. This is the most time consuming part of the calculation in the present study. In order to improve the accuracy of the later calculations, more dense distributions of $z_1^{(+)}(r)$ and $z_1^{(-)}(r)$ within the narrower interval of separation are preferable. This can be easily achieved by extending the total points of the matrix elements from 80 to 200 using an interpolation method. Then, for later convenience to compare with the MPM89 and MPM93 models, we use a formula derived from Eq. (50) to calculate contributions to the absorption coefficients (in dB/km) at the frequency $f = z_1^{(+)}(r) \times 29.979$ (in GHz) from all $z_1^{(+)}(r)$,

$$\alpha(f, T) = 2.026 \times 10^{-5} p_{\text{H}_2\text{O}} p_{\text{N}_2} \theta^3 f \mu^2 r^3 M_+ \times R_1^{(+)}(r) \frac{z_1^{(+)}(r)}{|r z_1'^{(+)}(r)|} e^{-\beta V_{\text{iso}}(r)} \rho_{\text{ani}}(r), \quad (54)$$

where $p_{\text{H}_2\text{O}}$ and p_{N_2} are pressures of H_2O and N_2 given in kPa, respectively, and $\theta \equiv 300/T$. In the above expression, μ and r are in atomic units, and all remaining factors including M_+ , $R_1^{(+)}(r)$, and $z_1^{(+)}(r)/|r z_1'^{(+)}(r)|$ are dimensionless.

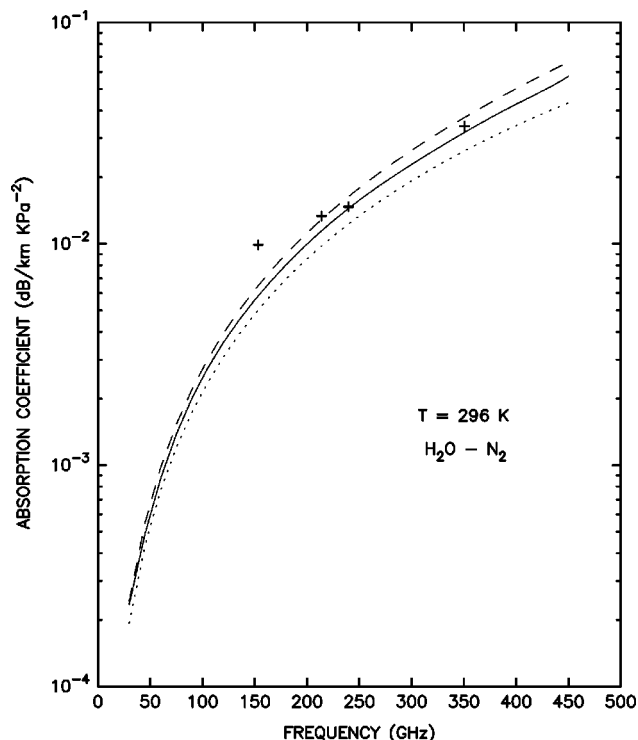


FIG. 6. The calculated $\text{H}_2\text{O}-\text{N}_2$ millimeter wave continuum (in units of dB/km kPa^{-2}) for $T=296$ K are represented by the solid line. The corresponding values derived from the MPM89 and MPM93 models are represented by the dotted and dashed lines, respectively. The values deduced from the Bauer *et al.* measurements at 153.000, 213.525, 239.370, and 350.300 GHz are represented by a +.

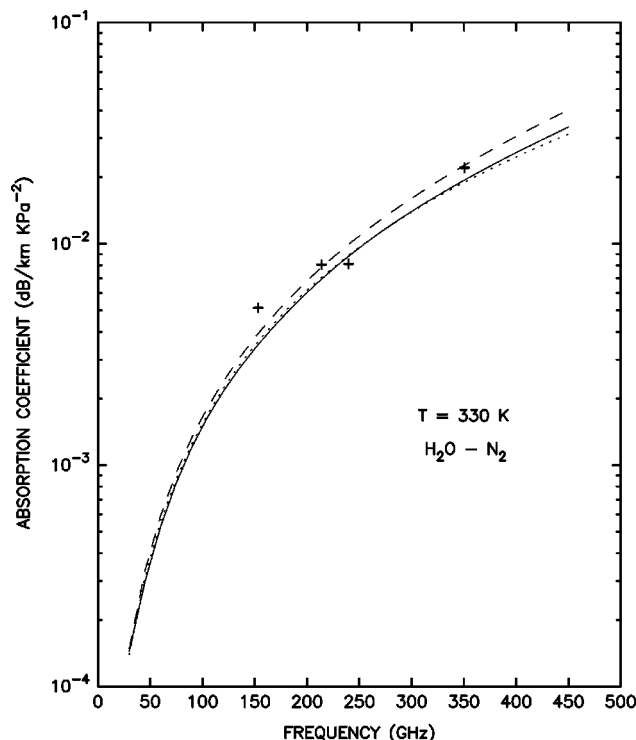


FIG. 7. The same as Fig. 6, except for $T=330$ K.

The formula used to calculate contributions from $z_1^{(-)}(r)$ is similar to Eq. (54), except for the replacement of M_+ by M_- and the replacement of the superscript (+) by (-).

There are several empirical models in current use for predicting the millimeter wave continuum of water vapor resulting from the buffer gas N_2 .^{9,10,18} Unfortunately, these empirical models differ significantly from each other. There are also a number of laboratory measurements carried out in millimeter windows,¹⁹⁻²⁴ but values of the foreign continuum deduced from measurements contain uncertainties because one has to subtract local line absorptions and the self-continuum from the raw data, and this procedure introduces errors. As a first attempt to explain the millimeter wave foreign continuum from first principles, it is not our intention here to make comprehensive comparisons with all models. Instead, we choose the MPM89 and MPM93 models as examples because they are well-known and widely used ones. With respect to measurements, we will compare our results with values deduced from the Bauer *et al.* data¹⁹⁻²² because the measurements were performed more recently and under more diverse conditions. We plot the calculated absorption coefficients of $\text{H}_2\text{O}-\text{N}_2$ below 450 GHz for $T=296$, 330, and 270 K in Figs. 6, 7, and 8, respectively, together with values derived from the MPM89 and MPM93 models. In Figs. 6 and 7, we also plot values obtained by subtracting local Van Vleck-Weisskopf line contributions up to 1000 GHz from the Bauer *et al.* measurements of $\text{H}_2\text{O}-\text{N}_2$ at 153.000, 213.525, 239.370, and 350.300 GHz,

respectively. As shown in these figures, the theoretical predictions are smooth functions of the frequency and they increase almost quadratically as the frequency increases. In comparison with the MPM89 and MPM93 models, our values lie between them. In addition, except for f

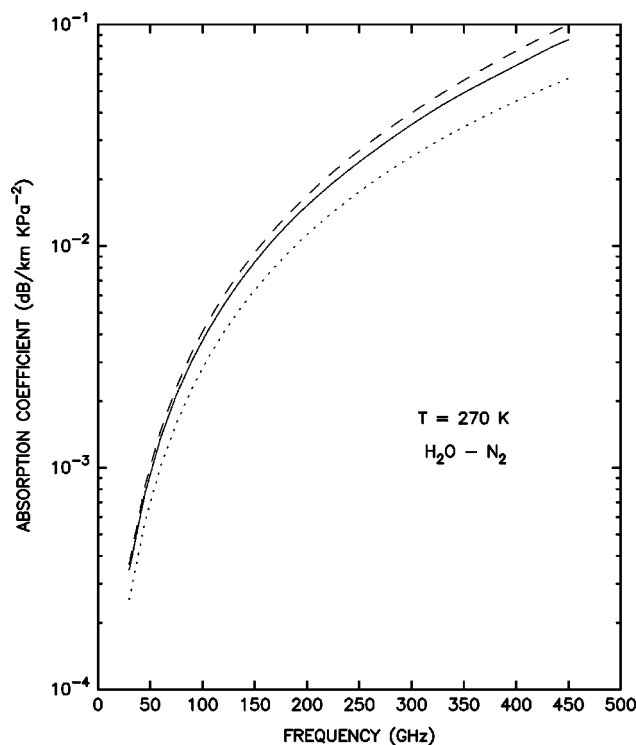


FIG. 8. The same as Fig. 6, except for $T=270$ K; no experimental data is available.

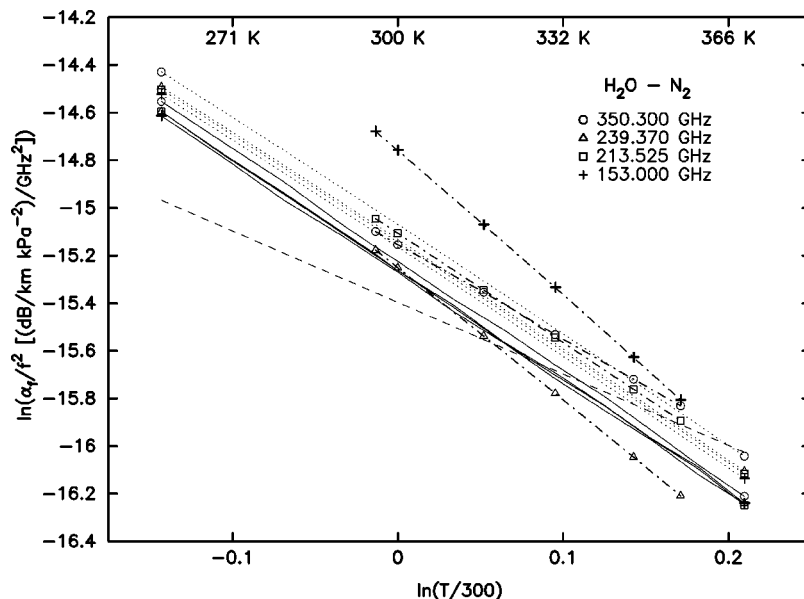


FIG. 9. A log-log plot of the calculated $\text{H}_2\text{O}-\text{N}_2$ millimeter wave continuum divided by the square of the frequency (in units of $\text{dB/km kPa}^{-2} \text{GHz}^{-2}$) at $f = 153.000, 213.525, 239.370$, and 350.300 GHz, respectively, as a function of the temperature. The theoretical values obtained at these frequencies are represented by the solid lines with different symbols $+$, \square , \triangle , and \circ marked at their ends, respectively. Those obtained from the MPM93 model are represented by the four dotted lines with similar end marks. Because the continuum of the MPM89 model is proportional to the square of the frequency, the corresponding values are presented by one dashed line. The values deduced from the Bauer *et al.* measurements at these frequencies are plotted with the symbols $+$, \square , \triangle , and \circ , respectively; for clarity, the same symbol is linked by the dot-dashed line.

$=153.000$ GHz, our values agree well with those from the Bauer *et al.* measurements. In order to show the temperature dependence more clearly for the four specified frequencies $f=153.000, 213.525, 239.370$, and 350.300 GHz, respectively, we calculate $\alpha(f,T)$ for $T=260, 270, \dots, 290, 296, 300, \dots, 370$ K and plot $\alpha(f,T)/f^2$ in Fig. 9. As shown in the figure, they are four straight lines; the first three are almost identical and the fourth is parallel with a little separation. This implies that the temperature dependence of $\alpha(f,T)$ can be well characterized by T^n , where the index n is a constant. On the other hand, the frequency dependence is not exactly quadratic, but very close. We also plot the corresponding values obtained from the MPM89 and MPM93 models, and those deduced from the measurements of Bauer *et al.* in the same figure. Because the MPM89 model is proportional to $f^2 T^{-3}$, it is represented by one straight line only. Meanwhile, each of the MPM93 model and the Bauer *et al.* data is represented by four lines. As shown in the figure, our results, those of Bauer *et al.*, and the MPM93 model exhibit a very similar negative temperature dependence, much stronger than the MPM89 model. Given the fact that the MPM89 and MPM93 models differ significantly from each other and values deduced from the Bauer *et al.* measurements contain uncertainties, we think that the agreement is satisfactory.

It may be helpful for others if we provide a simple analytic formula to represent the present work. By fitting our results calculated for a dozen different temperatures ranging from 220 to 330 K, an expression for the continuum (in dB/km), applicable for f up to 450 GHz and for T ranging from 220 to 330 K, we find

$$\alpha(f,T) = 1.9525 \times 10^{-7} p_{\text{H}_2\text{O}} p_{\text{N}_2} (300/T)^{4.6019} f^{2.0389}. \quad (55)$$

In the above expression, as expected, the frequency dependence of $\alpha(f,T)$ is very close to, but not exactly quadratic. Meanwhile, the temperature index obtained is a constant -4.6019 that differs significantly from -3 of the MPM89 model. It worth emphasizing that the above formula repre-

sents the present calculated continuum only. We think that further measurements will allow us to refine the theoretical results.

III. DISCUSSIONS AND CONCLUSIONS

Before we go further, we have to first answer a question: what are our calculated values from the Lanczos algorithm? In Figs. 6–9, we compare our results with the foreign-continuum component of the MPM89 and MPM93 models and values representing similar contributions from the Bauer *et al.* data. This implies tacitly that in the millimeter wave spectral region, our calculated absorptions contain the continuum of H_2O resulting from interacting with N_2 only, but not contributions from local H_2O lines. It is difficult for us to provide a rigorous verification of this assertion because we calculate the millimeter wave absorption resulting from the whole pure-rotational band of H_2O , as shown by the formalism presented above. But, based on our calculations, there are several arguments to support our conclusion. First of all, as shown by our derivation of the absorption with the Lanczos algorithm, the effect of the pure-rotational band is represented by contributions from poles. We have shown that if the H_2O molecule is isolated, up to the cutoff of the continued fractions used here, there are no poles within the millimeter spectral region. In fact, the nearest “pseudoline” for $T=296$ K is at 46.1918 cm^{-1} ($=1,385$ GHz). This means that within our formalism, there are no local lines located in the millimeter region and no corresponding millimeter wave absorption from them. As mentioned previously, the latter is not rigorously true, but is acceptable as an approximation. In contrast, the frequency of the nearest “pseudoline,” $1,385$ GHz, gives us a hint as to how to choose a cutoff when one adds local line contributions. Second, the calculated absorptions are a smooth function of the frequency and their values are proportional to a product of the pressures of H_2O and N_2 . Usually the absorptions resulting from local lines have sharp features. One may argue that the calculated absorptions

resulting from an average over the whole band could contain local line contributions if these lines are smeared completely and their absorptions are well smoothed in the averaging process. But, no matter how flat a line shape becomes, its integration over frequency remains unchanged. Thus, it is clear that such smeared absorptions are proportional to the pressure of H_2O only, independent of the pressure of N_2 . Therefore, we can conclude that the calculated millimeter wave absorption from the Lanczos algorithm represents the H_2O – N_2 continuum only. In order to obtain the total absorptions, one has to add the H_2O – H_2O continuum and extra local line absorptions. To obtain the latter is beyond the scope of the current formalism, but it can be easily calculated using a Van Vleck–Weisskopf line shape, as in the MPM89 and MPM93 models. We note that in these two models, there are 30 and 34 local lines included in the calculations, respectively, resulting from a choice of 1000 GHz cutoff. It is interesting to note that 1000 GHz is close to the nearest “pseudoline” frequency 1385 GHz derived here for $T = 296$ K. This provides, more or less, a justification for imposing the 1000 GHz cutoff in MPM89 and MPM93 models. One could extend the 1000 GHz cutoff if one adds the local line absorptions into the theoretical H_2O – N_2 continuum.

As mentioned above, our knowledge of the experimental millimeter wave foreign continuum is still somewhat uncertain. From the theoretical point of view, there are still debates going on about which mechanisms are responsible for this absorption. Besides the far-wing theory, CIA is a proposed candidate responsible for absorptions associated with the binary collisions.² Although one cannot rule out the possible significance of CIA, there are no quantitative CIA calculations so far. On the other hand, as shown by derivations given here in detail, we start from a sound physical basis and use the well-known Lanczos algorithm and the Monte Carlo method to perform numerical calculations. All assumptions and approximations involved have been carefully justified. Except for the interaction potential, there are no adjustable parameters. In addition, the same potential has been checked by comparing its predictions of the second virial coefficients at several temperatures with corresponding measurements. Given the fact that we are able to predict the magnitudes of the continuum and its negative temperature dependence, we conclude that one is able to explain this continuum without relying on appreciable CIA.

Concerning the far-wing line shape theory, we cannot directly say that the calculated results are from the far-wing contributions of individual lines because there are no line shapes involved in the present calculations. But, we can say that the present results are due to permanent dipole transitions of H_2O occurring in the presence of N_2 molecules. Therefore, both the effect of the whole band and the far-wing contributions from individual lines belong to the same physical mechanism. From the technical point view, of course, these two are not the same. They use different methods to account for contributions to the absorption from the permanent dipole transitions and pertain to different limitations. We think that in the millimeter spectral region, the present formalism is better than the far-wing line shape formalism because the latter’s applicability becomes questionable. Us-

ally, in the far-wing line shape formalism, one introduces the band average approximation by assuming that all the lines have a common shape, which represents an average over the band.⁴ This approximation is valid only in cases where in comparison with amounts by which the frequency of interest differs from strong lines, the latter are not widely distributed within the band. Because the frequencies of strong lines of the pure-rotational band with intensities at $T = 296$ K greater than $10^{-19} \text{ cm}^{-1}/(\text{molecule cm}^{-2})$ range from 36.6 to 374.5 cm^{-1} , this assumption is not true here. In addition, results obtained from the far-wing line shape theory could contain local structures resulting from nearby local lines in the millimeter spectral region, but the Lanczos formalism yields a completely smooth continuum that is more suitable for comparison with empirical models.

In the present study, we faced difficulties to evaluate matrix elements of operators such as $\mathcal{L}_1 \mathcal{L}_a^2 \mathcal{L}_1$ because the corresponding weighting functions oscillated wildly. It is well known that the typical representation of a Dirac delta function $\delta(x)$ looks like a very sharp peak located at $x = 0$ and the integration over x remains 1. However, it could have another representation that oscillates rapidly along the x axis but keeps its integration over x unchanged. In fact, Eq. (41) is an example and it has been used in evaluating a part of $+\langle 1 | \mathcal{L}_1 \mathcal{L}_a \mathcal{L}_1 | 1 \rangle_+$ analytically. Other distribution functions introduced in the present study look, more or less, like a Dirac delta function, but they are not. Some of them contain sharp peaks and others oscillate rapidly. The Monte Carlo method works well when weighting functions have sharp peaks, but it fails to yield reliable results with rapidly oscillating weighting functions. At present, we do not know how to deal with this case and we had to estimate their values. Of course, a better treatment is desirable.

We would like to make some comments about other possible improvements of the present work. In order to reduce the CPU time, we have assumed that the interaction potential contains cyclic coordinates. There are no fundamental problems to remove this restriction. In comparison with the present case, one of the main differences is that the distribution functions associated with H_2O become three-dimensional ones and the numbers of coefficients required to evaluate them increases dramatically.³ For example, for $J_{\text{max}} = 26$ it goes from 53 to 26 235. Another is that one has to carry out nine-dimensional integrations in calculating the matrix elements. All these are still manageable, but may require several days on a dozen CPUs. However, we do not expect that results derived from more general interaction potentials would differ dramatically from those presented here. Because the leading long-range dipole–quadrupole interaction is dominant and has been taken into account, differences between more general potentials and the one used here could be large only at short separations. But, these parts of potentials do not play an important role in the millimeter wave continuum absorption. An improvement could be made by including the higher-order long-range term, i.e., the quadrupole–quadrupole interaction of H_2O – N_2 in the calculations. Unfortunately, the latter does not contain cyclic coordinates, and it becomes necessary to perform the comprehensive calculations. In this case, we would prefer to choose

the more general site-site potential model because with the coordinate representation this does not introduce extra difficulty. Concerning the cutoff of the continued fraction, of course, one can go further to include more terms in Eq. (14). With the next higher-order cutoff, one needs to calculate another two matrix elements $\langle 1|\mathcal{L}^6|1\rangle$ and $\langle 1|\mathcal{L}^7|1\rangle$ because they appear in expressions for β_4^2 and α_4 . We think that one has to balance an improvement resulting from taking this step with other possible corrections at the current stage.

Finally, we would like to say that the present method could be used for other molecular systems, such as $\text{H}_2\text{O}-\text{CO}_2$ and $\text{H}_2\text{O}-\text{O}_2$, and the extension is straightforward. As an example, the density matrix of the CO_2 molecule was reported in our previous work.⁷ In comparison with the profile of the density matrix of N_2 shown in Fig. 1, the profile for CO_2 has sharper peaks and narrower widths because the rotational constant of CO_2 is much smaller than N_2 . In addition, the two peaks of CO_2 located at 0° and 180° are almost even, which results from the fact that there are no odd j ground states. Concerning the interaction of $\text{H}_2\text{O}-\text{CO}_2$, the dipole-quadrupole interaction is stronger than $\text{H}_2\text{O}-\text{N}_2$ because the quadrupole moment of CO_2 is about three times larger than N_2 . We expect that effects from all these differences will show up in the millimeter wave continuum. Given the fact that some measurements of $\text{H}_2\text{O}-\text{CO}_2$ are available,²⁵ it is worthwhile to apply this method for this system.

ACKNOWLEDGMENTS

This research was supported by the Biological and Environmental Research Program (BER), U.S. Department of Energy, Interagency Agreement No. DE-AI02-93ER61744 and by NASA through Grant NO. NAG5-8269. The authors would like to thank the National Energy Research Supercomputer (Livermore, CA) for computer time and facilities provided.

Also, we would like to thank Dr. A. Bauer for useful discussions.

- ¹P. W. Rosenkranz, *Radio Sci.* **33**, 919 (1998); **34**, 1025 (1999).
- ²A. Bauer and M. Godon, *J. Quant. Spectrosc. Radiat. Transf.* **69**, 277 (2001).
- ³Q. Ma and R. H. Tipping, *J. Chem. Phys.* **112**, 574 (2000); **116**, 4102 (2002).
- ⁴P. W. Rosenkranz, *J. Chem. Phys.* **83**, 6139 (1985); **87**, 163 (1987).
- ⁵E. Hudis, Y. Ben-Aryeh, and U. P. Oppenheim, *Phys. Rev. A* **43**, 3631 (1991); *J. Quant. Spectrosc. Radiat. Transf.* **47**, 319 (1992).
- ⁶Q. Ma and R. H. Tipping, *J. Chem. Phys.* **93**, 6127 (1990).
- ⁷Q. Ma and R. H. Tipping, *J. Chem. Phys.* **108**, 3386 (1998).
- ⁸Q. Ma and R. H. Tipping, *J. Chem. Phys.* **111**, 5909 (1999).
- ⁹H. J. Liebe, *Int. J. Infrared Millim. Waves* **10**, 631 (1989).
- ¹⁰H. J. Liebe, G. A. Hufford, and M. G. Cotton, *AGARD Conf. Proc.* 542, 1993, Secs. 3.1–3.10.
- ¹¹M. V. Tonkov and N. N. Filippov, *Opt. Spectrosc.* **50**, 144 (1981).
- ¹²G. Moro and J. H. Freed, in *Large Scale Eigenvalues Problems*, edited by J. Cullum and R. A. Willoughby (North-Holland, Amsterdam, 1986).
- ¹³*Analytic Theory of Continued Fractions*, edited by H. S. Wall (Van Nostrand, New York, 1948), p. 167.
- ¹⁴J. G. Parker, *Phys. Fluids* **2**, 449 (1959).
- ¹⁵S. A. Clough, Y. Beers, G. P. Klein, and L. S. Rothman, *J. Chem. Phys.* **59**, 2254 (1973).
- ¹⁶A. D. Buckingham, C. Graham, and J. H. Williams, *Mol. Phys.* **49**, 703 (1983).
- ¹⁷*The Virial Coefficients of Pure Gases and Mixtures*, edited by J. H. Dymond and E. B. Smith (Oxford University Press, Oxford, 1980).
- ¹⁸S. A. Clough, F. X. Kneizys, and R. W. Davies, *Atmos. Res.* **23**, 229 (1989).
- ¹⁹M. Godon, J. Carlier, and A. Bauer, *J. Quant. Spectrosc. Radiat. Transf.* **47**, 275 (1992).
- ²⁰A. Bauer, M. Godon, J. Carlier, Q. Ma, and R. H. Tipping, *J. Quant. Spectrosc. Radiat. Transf.* **50**, 463 (1993).
- ²¹A. Bauer, M. Godon, J. Carlier, and Q. Ma, *J. Quant. Spectrosc. Radiat. Transf.* **53**, 411 (1995).
- ²²T. Kuhn, A. Bauer, M. Godon, S. Bühler, and K. Künzi, *J. Quant. Spectrosc. Radiat. Transf.* **74**, 545 (2002).
- ²³H. J. Liebe, *Int. J. Infrared Millim. Waves* **5**, 207 (1984).
- ²⁴H. J. Liebe and D. H. Layton, NTIA Report, 87–224, Natl. Telecommun. and Inf. Admin., Boulder, Colorado, 1987.
- ²⁵A. Bauer, M. Godon, J. Carlier, and R. R. Gamache, *J. Mol. Spectrosc.* **176**, 45 (1996).